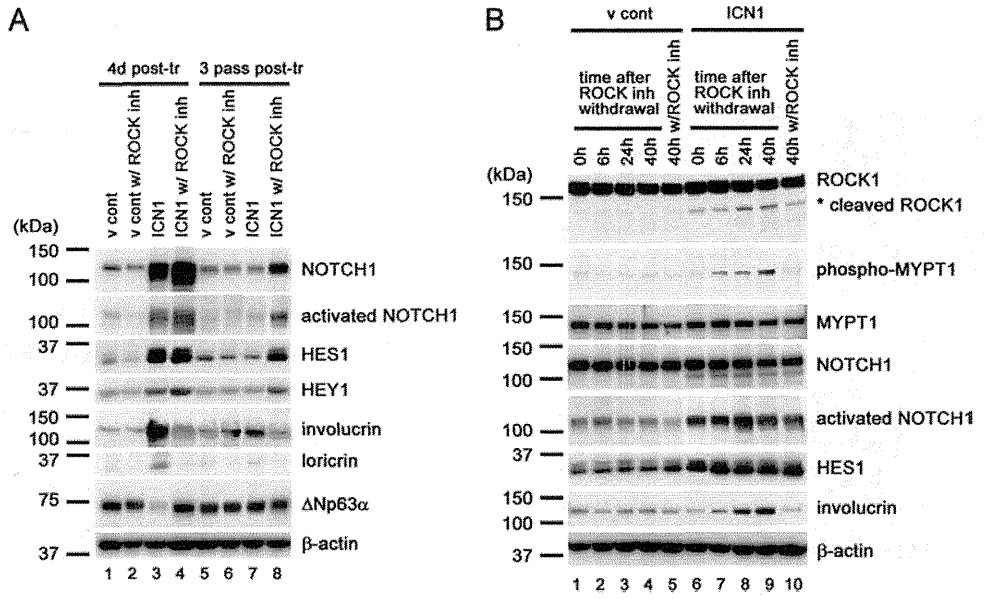

FIG 7 ROCK inhibition allows propagation of keratinocytes in the presence of constitutively active NOTCH1. (A) HCK1T cells pretreated with or without Y-27632 were transduced with the constitutively active form of NOTCH1 (ICN1) or vector control (v cont). Cells were cultivated until 22 days posttransduction (three passages) in the presence or absence of Y-27632. Cell extracts were prepared at 4 and 22 days posttransduction and subjected to immunoblotting analysis with the indicated antibodies. Note that the ROCK inhibitor inhibits differentiation and permits proliferation of ICN1-expressing cells. In contrast, control cells which have escaped after ICN1 transduction showed decreased levels of activated NOTCH1. (B) Cells were treated as for panel A. Cell lysates were prepared at the indicated time points after withdrawal of Y-27632 and subjected to immunoblotting analysis with the indicated antibodies.

It has been shown that the Rho inhibitor C3 as well as Y-27632 inhibited differentiation induced by single-cell suspension, although RhoA activity is unvaried during differentiation (35). In our monolayer culture model, conditional overexpression of a constitutively active form of RhoA was able to promote differentiation to some extent (Fig. 8B, lane 2). We then examined C3's effect on the process of keratinocyte differentiation. C3 only partially inhibited overall ROCK activation, judging from the phosphorylation levels of MYPT1 (Fig. 8C, compare lanes 2 and 7). Furthermore, this inhibition seemed to be closely associated with unexpected inhibition of the NOTCH1-caspase-ROCK1 axis through unknown mechanisms. Therefore, unlike keratinocyte differentiation induced by single-cell suspension assays, ROCK1 activation in monolayer culture essentially depends on its cleavage by caspase but not much on Rho activation, though we have not confirmed Rho activity during keratinocyte differentiation. These data support the conclusion that the NOTCH1-caspase-ROCK1 axis plays a major role in keratinocyte differentiation at least in monolayer culture. It is noteworthy that ROCK1 acts downstream of NOTCH1 but not NOTCH2, as ICN2 (a NOTCH2 intracellular form) did not induce ROCK1 cleavage and keratinocyte differentiation (Fig. 8A, compare lanes 2 and 4).

Proliferative defects upon dissociation in hiPSCs are partly attributable to NOTCH activity. It is well-known that human pluripotent stem cells such as hESCs undergo massive apoptosis when dissociated and that ROCK inhibitor treatment efficiently ameliorates such vulnerability to permit survival in clonal culture (39, 58). It is tempting to speculate that the NOTCH-ROCK pathway may also be activated in human pluripotent stem cells during the dissociation step with EDTA treatment and that this could be one mechanism underlying dissociation-induced loss of clonal growth potential. In an attempt to assess this possibility, we employed two lines of human induced pluripotent stem cells (hiPSCs). As shown in Fig. 9A and B, virtually no hiPSC colonies were formed from cells dissociated by trypsin-EDTA treatment, whereas NOTCH inhibition by a γ-secretase inhibitor partially restored the efficiency of colony formation to a degree comparable to that with Rho inhibitor C3-treated cells. Combination inhibition of γ-secretase and Rho had an additive effect on the clonogenic growth capacity to the same extent as ROCK inhibition, suggesting that the NOTCH-ROCK and the Rho-ROCK axis act in parallel in this cellular context.

In line with a previous study showing ROCK-dependent myosin activation as the direct cause of dissociation-induced cell death in hESCs (41), we also found that treatment with the myosin inhibitor blebbistatin showed equal efficacy as ROCK inhibition (Fig. 9C and D).

To substantiate further the link between NOTCH and ROCK in hiPSCs, we next assessed the status of NOTCH and ROCK in adherent small clumps of cells treated with EDTA. In accordance with the data with keratinocytes, EDTA treatment triggered immediate NOTCH1 activation accompanied by ROCK1 cleavage and MYPT1 phosphorylation (Fig. 10A, lanes 2 and 6). Importantly, treatment with a γ-secretase inhibitor resulted in abrogation of ROCK1 activation (Fig. 10A, lanes 4 and 8), suggesting that regulation of ROCK1 activity by NOTCH1 is also conserved in hiPSCs. Because EDTA treatment instigated drastic morphological change which was blocked by NOTCH or ROCK inhibition (Fig. 10B), we speculated that this stimulus may have an impact on the cell fate. Indeed, 3 days after EDTA treatment, expression of the stemness marker OCT3/4 was substantially downregulated in still-attached control cells (Fig. 10C, compare lanes 7 and 8). In-

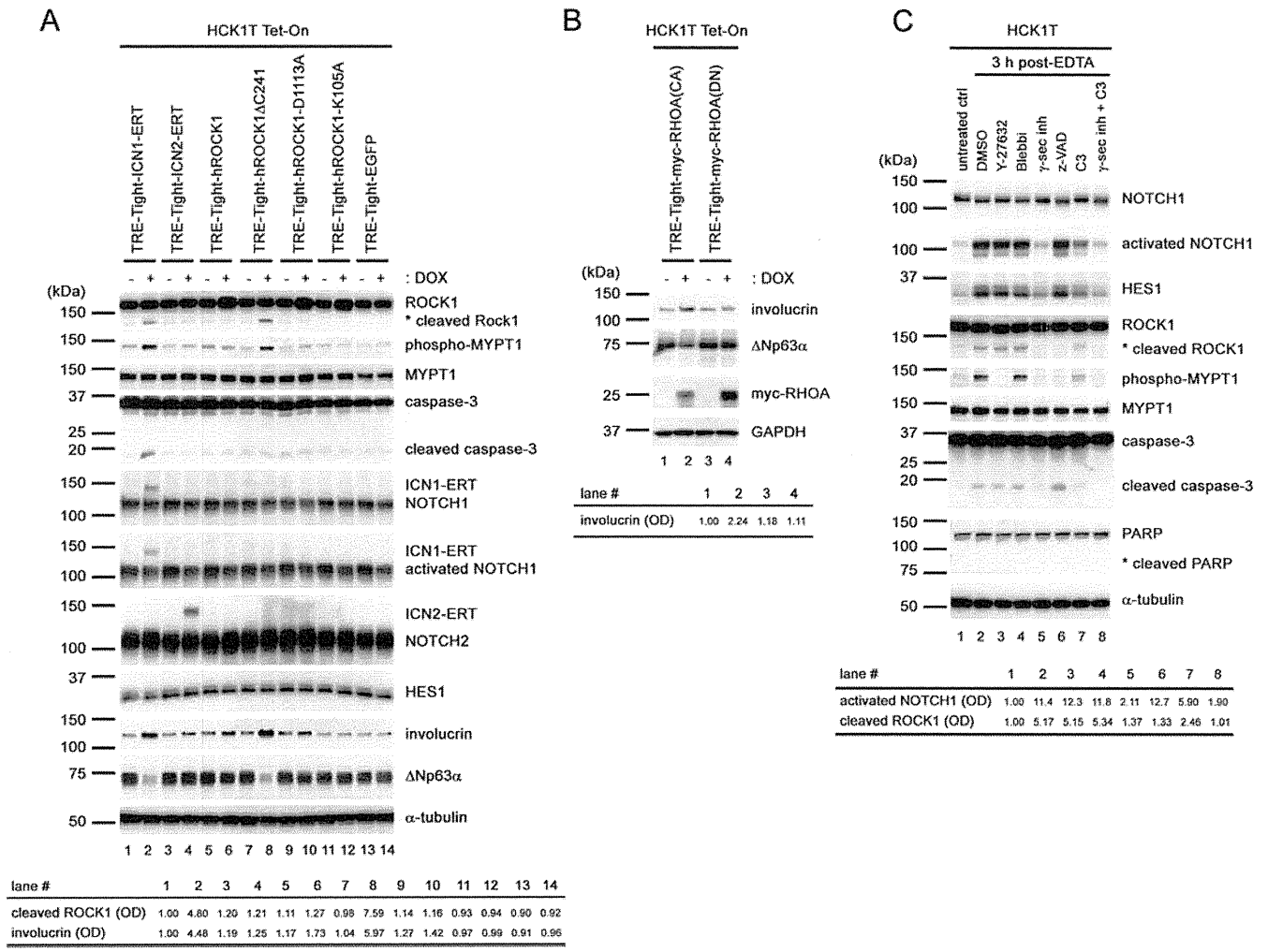

FIG 8 Ectopic expression of active ROCK1 induces keratinocyte differentiation. (A and B) HCK1T Tet-On cells were stably transduced with the indicated tetracycline-inducible gene constructs by retroviral gene transfer. Cells were either left untreated (−) or treated (+) with 1 μg/ml doxycycline (DOX) for 72 h. Cell extracts were analyzed by immunoblotting with the indicated antibodies. A long-exposed image for activated NOTCH1 is shown. Quantification of relative optical densities (OD) for the cleaved ROCK1 and involucrin bands, normalized to the value for the α-tubulin or GAPDH control, are indicated. (C) HCK1T cells, pretreated where indicated with 10 μM Y-27632, 10 μM blebbistatin, 10 μM γ-secretase inhibitor (DAPT), 20 μM z-VAD-fmk, or 1.0 μg/ml C3 for 3 h, were either left untreated or treated with 2.5 mM EDTA for 10 min and incubated with keratinocyte-SF medium for 3 h. Cell extracts were subjected to immunoblotting analysis with the indicated antibodies. Quantification of relative optical densities (OD) for the activated NOTCH1 and cleaved ROCK1 bands, normalized to the value for α-tubulin with the untreated control defined as 1, are indicated.

hibition of either NOTCH or Rho significantly prevented this transition (Fig. 10C). Of note, the inhibitor-treated colonies showed normal morphology in a mass, whereas the EDTA-treated controls exhibited heterogeneous and differentiated traits at this time point. These observations indicate that EDTA treatment induces acute ROCK1 activation and consequent loss of stemness at least partly in a NOTCH-dependent manner in hiPSCs.

DISCUSSION

Identification of NOTCH1 as a novel upstream regulator for ROCK1. The best-known upstream regulator for ROCK activity is Rho GTPase (32). In the normal cellular context, ROCK becomes an active kinase by conformational change through interaction with the GTP-bound form of Rho, which is thought to release the kinase domain from the carboxy-terminal autoinhibitory domain. In apoptotic cells, removal of the autoinhibitory domain of ROCK1 by caspase-3-mediated cleavage renders this protein constitutively active (54, 55, 59). In the present study, we first found that the cleaved ROCK1 is also generated immediately after emergence of the NOTCH1 intracellular form in the context of keratinocyte differentiation and revealed that activated NOTCH1 causes constitutive activation of ROCK1 through caspase cleavage upon EDTA treatment or exposure to differentiation-inducing stimuli such as serum as well as cell-cell contact (Fig. 11). We further demonstrated that this type of ROCK1 activation is mediated by a transcription-independent function of NOTCH1. Thus, we conclude that noncanonical NOTCH1 signaling triggers differentiation and a consequential decrease in clonogenicity mostly if not completely through ROCK1 activation in keratinocytes. To our knowledge, this is the first demonstration of NOTCH1 function as a novel and critical upstream regulator for ROCK1 activity. The Rho inhibitor C3 inhibited MYPT1 phosphorylation to some extent in concert with reduction of activated NOTCH1 and

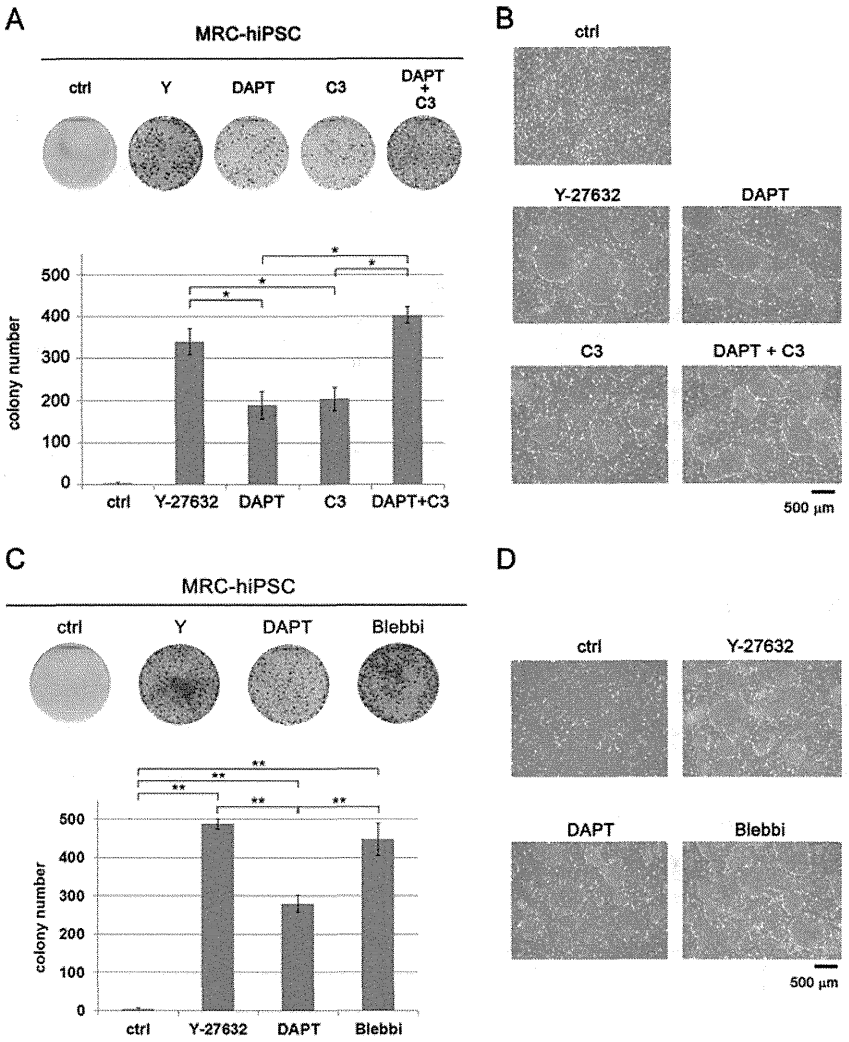

FIG 9 Activation of NOTCH and ROCK upon dissociation instigates loss of clonogenic growth capacity in hiPSCs. (A) MRC-hiPSCs, pretreated where indicated with 10 μM Y-27632 (Y) for 3 h, 10 μM DAPT for 3 h, 2.0 μg/ml C3 for 3 h, and 10 μM DAPT and 2.0 μg/ml C3 for 3 h, were completely dissociated by trypsin-EDTA treatment and pipetting. The dissociated cells were counted with Vi-CELL to confirm that the viabilities of each samples were greater than 90%, and aliquots of 2,000 cells were seeded on 60-mm dishes in the presence of MEF feeders. After 10 days of cultivation, the cells were stained with Giemsa's dye, and colonies were counted. The photographs are of representative dishes, and the graph illustrates means ± SDs. Treatment with any of these inhibitors significantly restored the clonal growth potential after dissociation. *, $P < 0.05$ according to Student's *t* tests. (B) Typical areas were photographed at 6 days postreplating. (C) MRC-hiPSCs, pretreated where indicated with 10 μM Y-27632 for 3 h, 10 μM DAPT for 3 h, and 10 μM blebbistatin for 3 h, were completely dissociated. The dissociated cells were seeded as for panel A, and colonies were counted. The photographs are of representative dishes, and the graph represents means ± SDs. **, $P < 0.01$ according to Student's *t* tests. (D) Typical areas were photographed at 6 days postreplating.

caspase-3 (Fig. 8C), implying a novel mechanism of ROCK inhibition by C3 independent of Rho inhibition. However, the mechanism underlying the inhibitory effect of C3 on NOTCH1 activation is currently unknown and awaits further investigation.

A recent report on the NOTCH1 nuclear interactome reveals ROCK1 as one of its interacting partners, raising the possibility of cross talk between these proteins (60). However, we have no evidence for interaction of the intracellular NOTCH1 proteins with caspase-3 and ROCK1 at present. Certainly, identification of a signaling mediator between NOTCH1 and ROCK1 warrants more research to provide a better understanding of this novel signaling pathway in cell biology. Interestingly, we failed to detect the intracellular form of NOTCH2 after differentiation induction, and ectopic expression of the NOTCH2 intracellular forms had a limited effect, if any, on ROCK1 cleavage and differentiation (Fig. 8A, lane 4), suggesting different regulatory mechanisms for activation and downstream signaling among NOTCH family members.

Functional diversity of caspases in cellular processes other than apoptosis has been described (61). In embryonic mouse keratinocytes, caspase-3 has been shown to be a transcriptional target of Notch1 and to have a role in high commitment to terminal differentiation (62). It is likely that ROCK1 activity is fostered by canonical NOTCH1 signaling through upregulation of caspase-3 gene expression. Because there is also a report showing that caspase-8 functions in epidermal homeostasis and regeneration through regulation of proliferation and inflammatory responses (63), we tested the possible involvement of caspase-8 in ROCK1 cleavage in differentiated keratinocytes. However, caspase-8 inhibition demonstrated little influence on activation of the

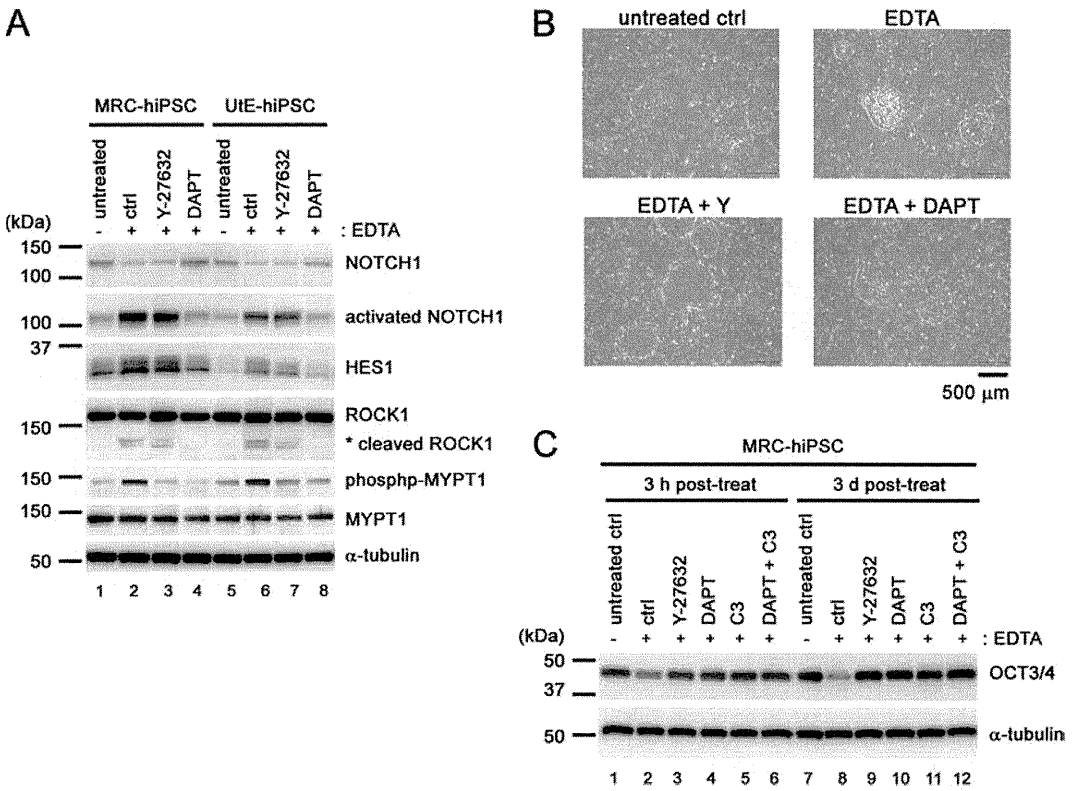

FIG 10 The defect in clonogenic growth upon dissociation in hiPSCs is partly attributable to NOTCH-dependent ROCK activation. (A) Adherent small clumps of MRC-hiPSCs and UtE-hiPSCs were pretreated with 10 μM Y-27632 for 3 h or 10 μM DAPT for 3 h and then either left untreated or treated with 2.5 mM EDTA in Hanks balanced salt solution without Ca^{2+} and Mg^{2+} [HBSS(−)] for 10 min at 37°C. After 3 h of incubation, hiPS cell extracts were prepared and subjected to immunoblotting analysis with the indicated antibodies. (B) Typical MRC-hiPSC colonies were photographed at 3 days after EDTA treatment. (C) Adherent small clumps of MRC-hiPSCs, pretreated where indicated with 10 μM Y-27632 for 3 h, 10 μM DAPT for 3 h, 2.0 μg/ml C3 for 3 h, and 10 μM DAPT and 2.0 μg/ml C3 for 3 h, were then either left untreated or treated with 2.5 mM EDTA. After 3 h and 3 days of cultivation, hiPS cell extracts were prepared and subjected to immunoblotting analysis.

NOTCH1-ROCK1 pathway and keratinocyte differentiation (unpublished observations), suggesting that activation of caspase-3 is unlikely to be mediated by caspase-8 downstream of NOTCH1.

Biological relevance of the NOTCH-ROCK pathway. In stratified epithelia such as the epidermis, cells in the basal layer constitute a proliferating population including stem cells and transit-amplifying cells. In the upper layer, differentiation-committed daughter cells are thought to arise by asymmetric cell division and then move toward the surface to undergo terminal differentiation (64). During the transition from the basal to the suprabasal layer, downregulation of p63, particularly its predominant isoform ΔNp63α, results in detachment from the basement membrane, at least partly via decreased expression of cell adhesion molecules (65). Downregulation of ΔNp63α also leads to upregulation of NOTCH1 gene expression and activity (9, 18). Having established that activated NOTCH1 triggers constitutive activation of ROCK1, we speculate that activated NOTCH1 may drive active movement of daughter cells toward the surface. This idea is supported by experiments showing that active ROCK1 induces formation of thick stress fibers and a cell contraction force which pushes cells upwards (54) and by the fact that Y-27632 inhibits differentiation as well as stratification in organotypic raft culture (37). Indeed, we observed that keratinocytes treated with EDTA exhibited increased cell motility and clambering movement, which were inhibited by Y-27632 (see Movies S1 and S2 in the supplemental material). We previously reported that ΔNp63α represses both p53-dependent and -independent expression of the Notch1 gene to support the proliferative capacity of normal human keratinocytes as well as a subset of cervical cancer cell lines (18). Thus, we propose that the p63-NOTCH1-ROCK1 axis plays an essential role in establishment of stratified epithelia through actomyosin-driven cell movement, though we cannot exclude the possible involvement of the Rho-ROCK pathway in this process. In terms of cancer biology, loss of p63 function is paradoxically associated with metastatic progression (66), implying another face of p63 as a tumor suppressor through the NOTCH1-ROCK1 pathway.

Two isoforms of ROCK, ROCK1 (ROKβ, p160ROCK) and ROCK2 (ROKα), have been identified in mammals; they share 65% overall identity and 92% identity in their kinase domains, and a number of lines of investigation have suggested nonoverlapping functions for these two isoforms (67–69). In this regard, ROCK1, but not ROCK2, has been shown to be constitutively activated by caspase-3 and to play roles in membrane blebbing during apoptosis (54, 55). We observed that knockdown of ROCK1 but not ROCK2 resulted in a reduced propensity for differentiation (Fig. 6B) and that a constitutively active form of ROCK1 induced differentiation (Fig. 8A). In parallel with our data, previous work has shown that the conditional expression of the activated form of ROCK2 also results in induction of differen-

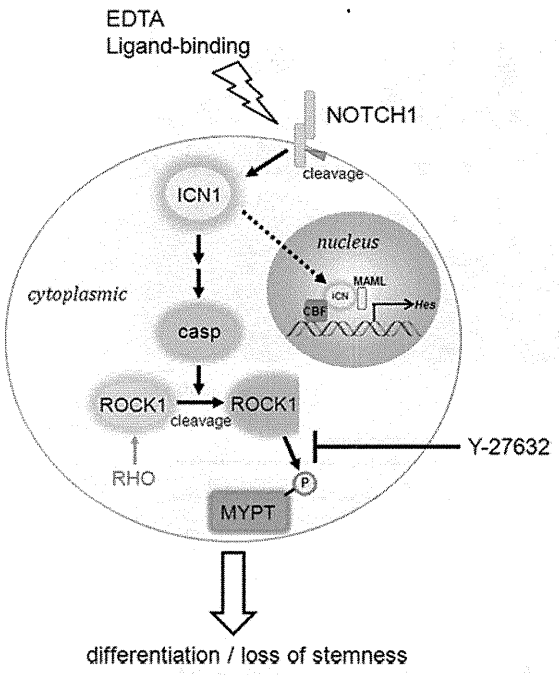

FIG 11 Proposed model for the NOTCH-ROCK pathway and its biological significance. NOTCH1 can be activated by dissociation of cells with EDTA as well as physiological ligand binding. The cytoplasmic form of NOTCH1, independent of its transcriptional activity, triggers caspase-mediated cleavage (activation) of ROCK1 by an as-yet-unknown mechanism. ROCK1 activation drives actomyocin reorganization through MYPT phosphorylation which results in cell differentiation or loss of stemness. The ROCK inhibitor Y-27632 blocks this pathway so as to inhibit differentiation of keratinocytes and maintain stemness of hiPSCs, as shown in this study.

tiation markers in keratinocytes (35). In contrast, it was reported that a ROCK inhibitor accelerated calcium- or suspension-induced keratinocyte differentiation (70). More recently, Notch1 was reported to be a p53 target gene involved in human keratinocyte tumor suppression through negative regulation of ROCK1,2 and MRCKalpha kinases (56). Furthermore, an oncogenic aspect of ROCK2 has also been reported (52, 71, 72). Apparent anomalies between these studies and our results imply complexity of the signals downstream of ROCK1 and ROCK2. However, our results clearly demonstrate that prompt activation of ROCK1 by noncanonical NOTCH1 signaling promotes keratinocyte differentiation and limits clonogenic cell growth. Part of the discrepancies may be explained by the use of different experimental systems. Our experimental system focused on early stages of keratinocyte differentiation in monolayer culture. However, our results are consistent with a more recent report that ROCK inhibition blocks differentiation as well as stratification in organotypic raft culture (37). It is possible that the canonical NOTCH1 signal and transcriptional repression of ROCK1,2 plays different roles in later stages of differentiation or tumor formation.

In spite of these important functions of ROCK1,2 in keratinocyte differentiation, no abnormalities in the epidermis of either Rock1- or Rock2-null mice have been described (67, 68, 73, 74). This suggests functional redundancy and compensatory mechanisms for these two proteins, though they show apparently quite different functions in culture. Synthetic effects in mice with compound heterozygous and/or homozygous disruptions in the Rock1 and Rock2 genes need to be delineated in detail.

Technical implications of NOTCH-ROCK dysregulation during cell passage. Our data show that keratinocytes of different tissue origins as well as hiPSCs exhibiting epiblast-like cell states have a conserved NOTCH1-ROCK1 pathway and that NOTCH activation is at least partly responsible for impaired clonogenicity upon dissociation with EDTA (Fig. 1C, 9, and 10). ROCK inhibition could robustly restore the proliferation capacity and contribute to the maintenance of stemness through blockade of cellular differentiation and/or apoptosis, unscheduled biological outcomes imposed by the EDTA treatment in cell culture. A recent groundbreaking report provided evidence that the combination of a ROCK inhibitor and fibroblast feeders indefinitely extends the life spans of many different types of human epithelial cells (38). Thus, it is highly likely that dissociation of cells with EDTA activates the NOTCH1-ROCK1 pathway and adversely affects the proliferative capacity of a broad spectrum of normal epithelial cells. Furthermore, most cell lines established through such procedures may represent a selected population resistant to the activation of the NOTCH-ROCK pathway.

In conclusion, our present study unveiled a link between noncanonical NOTCH signaling and ROCK activation and revealed a previously unrecognized function of NOTCH1 as a critical regulator of ROCK1 in dictating the cell fate. Our findings also imply a possible pitfall in cell culture and delineate a molecular rationale for the beneficial effects of the ROCK inhibitor Y-27632 in cultivating various cell types.

ACKNOWLEDGMENTS

We thank H. Sakaguchi, R. Sakamoto, M. Yamazaki, T. Ishiyama, and A. Noguchi for their expert technical assistance and H. Miyoshi for lentiviral constructs.

This work was supported in part by a Grant-in-Aid for Scientific Research from the Ministry of Education, Culture, Sports, Science, and Technology of Japan (to T. Yugawa) and by grant 23-B1 from the National Cancer Center Research and Development Fund and a Grant-in-Aid for Cancer Research from the Ministry of Health Labor and Welfare of Japan (to T. Kiyono).

T.Y. conceived the project, designed, performed, and analyzed experiments, and wrote the manuscript. K.N. performed the hiPSC clonogenic assay. N.G. and S.-I.O. provided cDNA clones and performed plasmid construction, respectively. M.F., A.U., and T.N. discussed and gave important advice on some experiments. T.K. participated in the experimental design and performed experiments.

We declare no conflict of interest related to this work.

REFERENCES

1. Lai EC. 2004. Notch signaling: control of cell communication and cell fate. Development 131:965–973.
2. Bray SJ. 2006. Notch signalling: a simple pathway becomes complex. Nat. Rev. Mol. Cell Biol. 7:678–689.
3. Kopan R, Ilagan MX. 2009. The canonical Notch signaling pathway: unfolding the activation mechanism. Cell 137:216–233.
4. Roy M, Pear WS, Aster JC. 2007. The multifaceted role of Notch in cancer. Curr. Opin. Genet. Dev. 17:52–59.
5. Koch U, Radtke F. 2007. Notch and cancer: a double-edged sword. Cell. Mol. Life Sci. 64:2746–2762.
6. Talora C, Campese AF, Bellavia D, Felli MP, Vacca A, Gulino A, Screpanti I. 2008. Notch signaling and diseases: an evolutionary journey from a simple beginning to complex outcomes. Biochim. Biophys. Acta 1782:489–497.
7. South AP, Cho RJ, Aster JC. 2012. The double-edged sword of Notch signaling in cancer. Semin. Cell Dev. Biol. 23:458–464.
8. Watt FM, Estrach S, Ambler CA. 2008. Epidermal Notch signalling: differentiation, cancer and adhesion. Curr. Opin. Cell Biol. 20:171–179.

9. Dotto GP. 2009. Crosstalk of Notch with p53 and p63 in cancer growth control. Nat. Rev. Cancer 9:587–595.
10. Tan MJ, White EA, Sowa ME, Harper JW, Aster JC, Howley PM. 2012. Cutaneous beta-human papillomavirus E6 proteins bind Mastermind-like coactivators and repress Notch signaling. Proc. Natl. Acad. Sci. U. S. A. 109:E1473–E1480.
11. Lowell S, Jones P, Le Roux I, Dunne J, Watt FM. 2000. Stimulation of human epidermal differentiation by delta-notch signalling at the boundaries of stem-cell clusters. Curr. Biol. 10:491–500.
12. Nicolas M, Wolfer A, Raj K, Kummer JA, Mill P, van Noort M, Hui CC, Clevers H, Dotto GP, Radtke F. 2003. Notch1 functions as a tumor suppressor in mouse skin. Nat. Genet. 33:416–421.
13. Kolly C, Suter MM, Muller EJ. 2005. Proliferation, cell cycle exit, and onset of terminal differentiation in cultured keratinocytes: pre-programmed pathways in control of C-Myc and Notch1 prevail over extracellular calcium signals. J. Invest. Dermatol. 124:1014–1025.
14. Yugawa T, Handa K, Narisawa-Saito M, Ohno S, Fujita M, Kiyono T. 2007. Regulation of Notch1 gene expression by p53 in epithelial cells. Mol. Cell. Biol. 27:3732–3742.
15. Miller AC, Lyons EL, Herman TG. 2009. cis-inhibition of Notch by endogenous Delta biases the outcome of lateral inhibition. Curr. Biol. 19:1378–1383.
16. Fleming RJ, Hori K, Sen A, Filloramo GV, Langer JM, Obar RA, Artavanis-Tsakonas S, Maharaj-Best AC. 2013. An extracellular region of Serrate is essential for ligand-induced cis-inhibition of Notch signaling. Development 140:2039–2049.
17. Sprinzak D, Lakhanpal A, Lebon L, Santat LA, Fontes ME, Anderson GA, Garcia-Ojalvo J, Elowitz MB. 2010. cis-interactions between Notch and Delta generate mutually exclusive signalling states. Nature 465:86–90.
18. Yugawa T, Narisawa-Saito M, Yoshimatsu Y, Haga K, Ohno S, Egawa N, Fujita M, Kiyono T. 2010. DeltaNp63alpha repression of the Notch1 gene supports the proliferative capacity of normal human keratinocytes and cervical cancer cells. Cancer Res. 70:4034–4044.
19. Mills AA, Zheng B, Wang XJ, Vogel H, Roop DR, Bradley A. 1999. p63 is a p53 homologue required for limb and epidermal morphogenesis. Nature 398:708–713.
20. Yang A, Schweitzer R, Sun D, Kaghad M, Walker N, Bronson RT, Tabin C, Sharpe A, Caput D, Crum C, McKeon F. 1999. p63 is essential for regenerative proliferation in limb, craniofacial and epithelial development. Nature 398:714–718.
21. Nguyen BC, Lefort K, Mandinova A, Antonini D, Devgan V, Della Gatta G, Koster MI, Zhang Z, Wang J, Tommasi di Vignano A, Kitajewski J, Chiorino G, Roop DR, Missero C, Dotto GP. 2006. Cross-regulation between Notch and p63 in keratinocyte commitment to differentiation. Genes Dev. 20:1028–1042.
22. Yi R, Poy MN, Stoffel M, Fuchs E. 2008. A skin microRNA promotes differentiation by repressing 'stemness'. Nature 452:225–229.
23. Lena AM, Shalom-Feuerstein R, Rivetti di Val Cervo P, Aberdam D, Knight RA, Melino G, Candi E. 2008. miR-203 represses 'stemness' by repressing DeltaNp63. Cell Death Differ. 15:1187–1195.
24. Melino G, Gallagher E, Aqeilan RI, Knight R, Peschiaroli A, Rossi M, Scialpi F, Malatesta M, Zocchi L, Browne G, Ciechanover A, Bernassola F. 2008. Itch: a HECT-type E3 ligase regulating immunity, skin and cancer. Cell Death Differ. 15:1103–1112.
25. Rand MD, Grimm LM, Artavanis-Tsakonas S, Patriub V, Blacklow SC, Sklar J, Aster JC. 2000. Calcium depletion dissociates and activates heterodimeric notch receptors. Mol. Cell. Biol. 20:1825–1835.
26. Gupta-Rossi N, Le Bail O, Gonen H, Brou C, Logeat F, Six E, Ciechanover A, Israel A. 2001. Functional interaction between SEL-10, an F-box protein, and the nuclear form of activated Notch1 receptor. J. Biol. Chem. 276:34371–34378.
27. Krejci A, Bray S. 2007. Notch activation stimulates transient and selective binding of Su(H)/CSL to target enhancers. Genes Dev. 21:1322–1327.
28. van Tetering G, van Diest P, Verlaan I, van der Wall E, Kopan R, Vooijs M. 2009. Metalloprotease ADAM10 is required for Notch1 site 2 cleavage. J. Biol. Chem. 284:31018–31027.
29. Perumalsamy LR, Marcel N, Kulkarni S, Radtke F, Sarin A. 2012. Distinct spatial and molecular features of notch pathway assembly in regulatory T cells. Sci. Signal. 5:ra53. doi:10.1126/scisignal.2002859.
30. Sanalkumar R, Dhanesh SB, James J. 2010. Non-canonical activation of Notch signaling/target genes in vertebrates. Cell. Mol. Life Sci. 67:2957–2968.
31. Andersen P, Uosaki H, Shenje LT, Kwon C. 2012. Non-canonical Notch signaling: emerging role and mechanism. Trends Cell Biol. 22:257–265.
32. Jaffe AB, Hall A. 2005. Rho GTPases: biochemistry and biology. Annu. Rev. Cell Dev. Biol. 21:247–269.
33. Riento K, Ridley AJ. 2003. Rocks: multifunctional kinases in cell behaviour. Nat. Rev. Mol. Cell Biol. 4:446–456.
34. Narumiya S, Tanji M, Ishizaki T. 2009. Rho signaling, ROCK and mDia1, in transformation, metastasis and invasion. Cancer Metastasis Rev. 28:65–76.
35. McMullan R, Lax S, Robertson VH, Radford DJ, Broad S, Watt FM, Rowles A, Croft DR, Olson MF, Hotchin NA. 2003. Keratinocyte differentiation is regulated by the Rho and ROCK signaling pathway. Curr. Biol. 13:2185–2189.
36. Liebig T, Erasmus J, Kalaji R, Davies D, Loirand G, Ridley A, Braga VM. 2009. RhoE Is required for keratinocyte differentiation and stratification. Mol. Biol. Cell 20:452–463.
37. Chapman S, Liu X, Meyers C, Schlegel R, McBride AA. 2010. Human keratinocytes are efficiently immortalized by a Rho kinase inhibitor. J. Clin. Invest. 120:2619–2626.
38. Liu X, Ory V, Chapman S, Yuan H, Albanese C, Kallakury B, Timofeeva OA, Nealon C, Dakic A, Simic V, Haddad BR, Rhim JS, Dritschilo A, Riegel A, McBride A, Schlegel R. 2012. ROCK inhibitor and feeder cells induce the conditional reprogramming of epithelial cells. Am. J. Pathol. 180:599–607.
39. Watanabe K, Ueno M, Kamiya D, Nishiyama A, Matsumura M, Wataya T, Takahashi JB, Nishikawa S, Muguruma K, Sasai Y. 2007. A ROCK inhibitor permits survival of dissociated human embryonic stem cells. Nat. Biotechnol. 25:681–686.
40. Chen G, Hou Z, Gulbranson DR, Thomson JA. 2010. Actin-myosin contractility is responsible for the reduced viability of dissociated human embryonic stem cells. Cell Stem Cell 7:240–248.
41. Ohgushi M, Matsumura M, Eiraku M, Murakami K, Aramaki T, Nishiyama A, Muguruma K, Nakano T, Suga H, Ueno M, Ishizaki T, Suemori H, Narumiya S, Niwa H, Sasai Y. 2010. Molecular pathway and cell state responsible for dissociation-induced apoptosis in human pluripotent stem cells. Cell Stem Cell 7:225–239.
42. Ohgushi M, Sasai Y. 2011. Lonely death dance of human pluripotent stem cells: ROCKing between metastable cell states. Trends Cell Biol. 21: 274–282.
43. Jacobs JP, Jones CM, Baille JP. 1970. Characteristics of a human diploid cell designated MRC-5. Nature 227:168–170.
44. Cui CH, Uyama T, Miyado K, Terai M, Kyo S, Kiyono T, Umezawa A. 2007. Menstrual blood-derived cells confer human dystrophin expression in the murine model of Duchenne muscular dystrophy via cell fusion and myogenic transdifferentiation. Mol. Biol. Cell 18:1586–1594.
45. Takahashi K, Tanabe K, Ohnuki M, Narita M, Ichisaka T, Tomoda K, Yamanaka S. 2007. Induction of pluripotent stem cells from adult human fibroblasts by defined factors. Cell 131:861–872.
46. Nishino K, Toyoda M, Yamazaki-Inoue M, Makino H, Fukawatase Y, Chikazawa E, Takahashi Y, Miyagawa Y, Okita H, Kiyokawa N, Akutsu H, Umezawa A. 2010. Defining hypo-methylated regions of stem cell-specific promoters in human iPS cells derived from extra-embryonic amnions and lung fibroblasts. PLoS One 5:e13017. doi:10.1371/journal.pone.0013017.
47. Nishino K, Toyoda M, Yamazaki-Inoue M, Fukawatase Y, Chikazawa E, Sakaguchi H, Akutsu H, Umezawa A. 2011. DNA methylation dynamics in human induced pluripotent stem cells over time. PLoS Genet. 7:e1002085. doi:10.1371/journal.pgen.1002085.
48. Weng AP, Nam Y, Wolfe MS, Pear WS, Griffin JD, Blacklow SC, Aster JC. 2003. Growth suppression of pre-T acute lymphoblastic leukemia cells by inhibition of notch signaling. Mol. Cell. Biol. 23:655–664.
49. Mandinova A, Lefort K, Tommasi di Vignano A, Stonely W, Ostano P, Chiorino G, Iwaki H, Nakanishi J, Dotto GP. 2008. The FoxO3a gene is a key negative target of canonical Notch signalling in the keratinocyte UVB response. EMBO J. 27:1243–1254.
50. Narisawa-Saito M, Yoshimatsu Y, Ohno S, Yugawa T, Egawa N, Fujita M, Hirohashi S, Kiyono T. 2008. An in vitro multistep carcinogenesis model for human cervical cancer. Cancer Res. 68:5699–5705.
51. Ongusaha PP, Kim HG, Boswell SA, Ridley AJ, Der CJ, Dotto GP, Kim YB, Aaronson SA, Lee SW. 2006. RhoE is a pro-survival p53 target gene that inhibits ROCK I-mediated apoptosis in response to genotoxic stress. Curr. Biol. 16:2466–2472.
52. Wong CC, Wong CM, Tung EK, Man K, Ng IO. 2009. Rho-kinase 2 is

frequently overexpressed in hepatocellular carcinoma and involved in tumor invasion. Hepatology **49**:1583–1594.
53. **Weng AP, Ferrando AA, Lee W, Morris JPt Silverman LB, Sanchez-Irizarry C, Blacklow SC, Look AT, Aster JC.** 2004. Activating mutations of NOTCH1 in human T cell acute lymphoblastic leukemia. Science **306**: 269–271.
54. **Coleman ML, Sahai EA, Yeo M, Bosch M, Dewar A, Olson MF.** 2001. Membrane blebbing during apoptosis results from caspase-mediated activation of ROCK I. Nat. Cell Biol. **3**:339–345.
55. **Sebbagh M, Renvoize C, Hamelin J, Riche N, Bertoglio J, Breard J.** 2001. Caspase-3-mediated cleavage of ROCK I induces MLC phosphorylation and apoptotic membrane blebbing. Nat. Cell Biol. **3**:346–352.
56. **Lefort K, Mandinova A, Ostano P, Kolev V, Calpini V, Kolfschoten I, Devgan V, Lieb J, Raffoul W, Hohl D, Neel V, Garlick J, Chiorino G, Dotto GP.** 2007. Notch1 is a p53 target gene involved in human keratinocyte tumor suppression through negative regulation of ROCK1/2 and MRCKalpha kinases. Genes Dev. **21**:562–577.
57. **Ronchini C, Capobianco AJ.** 2000. Notch(ic)-ER chimeras display hormone-dependent transformation, nuclear accumulation, phosphorylation and CBF1 activation. Oncogene **19**:3914–3924.
58. **Krawetz RJ, Li X, Rancourt DE.** 2009. Human embryonic stem cells: caught between a ROCK inhibitor and a hard place. Bioessays **31**:336–343.
59. **Chang J, Xie M, Shah VR, Schneider MD, Entman ML, Wei L, Schwartz RJ.** 2006. Activation of Rho-associated coiled-coil protein kinase 1 (ROCK-1) by caspase-3 cleavage plays an essential role in cardiac myocyte apoptosis. Proc. Natl. Acad. Sci. U. S. A. **103**:14495–14500.
60. **Yatim A, Benne C, Sobhian B, Laurent-Chabalier S, Deas O, Judde JG, Lelievre JD, Levy Y, Benkirane M.** 2012. NOTCH1 nuclear interactome reveals key regulators of its transcriptional activity and oncogenic function. Mol. Cell **48**:445–458.
61. **Yi CH, Yuan J.** 2009. The Jekyll and Hyde functions of caspases. Dev. Cell **16**:21–34.
62. **Okuyama R, Nguyen BC, Talora C, Ogawa E, Tommasi di Vignano A, Lioumi M, Chiorino G, Tagami H, Woo M, Dotto GP.** 2004. High commitment of embryonic keratinocytes to terminal differentiation through a Notch1-caspase 3 regulatory mechanism. Dev. Cell **6**:551–562.
63. **Lee P, Lee DJ, Chan C, Chen SW, Ch'en I, Jamora C.** 2009. Dynamic expression of epidermal caspase 8 simulates a wound healing response. Nature **458**:519–523.
64. **Blanpain C, Fuchs E.** 2009. Epidermal homeostasis: a balancing act of stem cells in the skin. Nat. Rev. Mol. Cell Biol. **10**:207–217.
65. **Carroll DK, Carroll JS, Leong CO, Cheng F, Brown M, Mills AA, Brugge JS, Ellisen LW.** 2006. p63 regulates an adhesion programme and cell survival in epithelial cells. Nat. Cell Biol. **8**:551–561.
66. **Melino G.** 2011. p63 is a suppressor of tumorigenesis and metastasis interacting with mutant p53. Cell Death Differ. **18**:1487–1499.
67. **Thumkeo D, Keel J, Ishizaki T, Hirose M, Nonomura K, Oshima H, Oshima M, Taketo MM, Narumiya S.** 2003. Targeted disruption of the mouse rho-associated kinase 2 gene results in intrauterine growth retardation and fetal death. Mol. Cell. Biol. **23**:5043–5055.
68. **Shimizu Y, Thumkeo D, Keel J, Ishizaki T, Oshima H, Oshima M, Noda Y, Matsumura F, Taketo MM, Narumiya S.** 2005. ROCK-I regulates closure of the eyelids and ventral body wall by inducing assembly of actomyosin bundles. J. Cell Biol. **168**:941–953.
69. **Lock FE, Hotchin NA.** 2009. Distinct roles for ROCK1 and ROCK2 in the regulation of keratinocyte differentiation. PLoS One **4**:e8190. doi:10.1371/journal.pone.0008190.
70. **Grossi M, Hiou-Feige A, Tommasi Di Vignano A, Calautti E, Ostano P, Lee S, Chiorino G, Dotto GP.** 2005. Negative control of keratinocyte differentiation by Rho/CRIK signaling coupled with up-regulation of KyoT1/2 (FHL1) expression. Proc. Natl. Acad. Sci. U. S. A. **102**:11313–11318.
71. **Zheng S, Huang J, Zhou K, Zhang C, Xiang Q, Tan Z, Wang T, Fu X.** 2011. 17beta-Estradiol enhances breast cancer cell motility and invasion via extra-nuclear activation of actin-binding protein ezrin. PLoS One **6**:e22439. doi:10.1371/journal.pone.0022439.
72. **Vega FM, Fruhwirth G, Ng T, Ridley AJ.** 2011. RhoA and RhoC have distinct roles in migration and invasion by acting through different targets. J. Cell Biol. **193**:655–665.
73. **Zhang YM, Bo J, Taffet GE, Chang J, Shi J, Reddy AK, Michael LH, Schneider MD, Entman ML, Schwartz RJ, Wei L.** 2006. Targeted deletion of ROCK1 protects the heart against pressure overload by inhibiting reactive fibrosis. FASEB J. **20**:916–925.
74. **Lee DH, Shi J, Jeoung NH, Kim MS, Zabolotny JM, Lee SW, White MF, Wei L, Kim YB.** 2009. Targeted disruption of ROCK1 causes insulin resistance in vivo. J. Biol. Chem. **284**:11776–11780.

HERPESVIRIDAE

RESEARCH Open Access

Human cytomegalovirus induces apoptosis in neural stem/progenitor cells derived from induced pluripotent stem cells by generating mitochondrial dysfunction and endoplasmic reticulum stress

Hiroyuki Nakamura[1*], Huanan Liao[1], Kahori Minami[2], Masashi Toyoda[2], Hidenori Akutsu[2], Yoshitaka Miyagawa[3], Hajime Okita[3], Nobutaka Kiyokawa[3], Akihiro Umezawa[2], Ken-Ichi Imadome[1], Naoki Inoue[4] and Shigeyoshi Fujiwara[1]

Abstract

Background: Congenital human cytomegalovirus (HCMV) infection, a leading cause of birth defects, is most often manifested as neurological disorders. The pathogenesis of HCMV-induced neurological disorders is, however, largely unresolved, primarily because of limited availability of model systems to analyze the effects of HCMV infection on neural cells.

Methods: An induced pluripotent stem cell (iPSC) line was established from the human fibroblast line MRC5 by introducing the Yamanaka's four factors and then induced to differentiate into neural stem/progenitor cells (NSPCs) by dual inhibition of the SMAD signaling pathway using Noggin and SB-431542.

Results: iPSC-derived NSPCs (NSPC/iPSCs) were susceptible to HCMV infection and allowed the expression of both early and late viral gene products. HCMV-infected NSPC/iPSCs underwent apoptosis with the activation of caspase-3 and −9 as well as positive staining by the terminal deoxynucleotidyl transferase-mediated dUTP nick-end labeling (TUNEL). Cytochrome c release from mitochondria to cytosol was observed in these cells, indicating the involvement of mitochondrial dysfunction in their apoptosis. In addition, phosphorylation of proteins involved in the unfolded protein response (UPR), such as PKR-like eukaryotic initiation factor 2a kinase (PERK), c-Jun NH2-terminal kinase (JNK), inositol-requiring enzyme 1 (IRE1), and the alpha subunit of eukaryotic initiation factor 2 (eIF2α) was observed in HCMV-infected NSPC/iPSCs. These results, coupled with the finding of increased expression of mRNA encoding the C/EBP-homologous protein (CHOP) and the detection of a spliced form of X-box binding protein 1 (XBP1) mRNA, suggest that endoplasmic reticulum (ER) stress is also involved in HCMV-induced apoptosis of these cells.

Conclusions: iPSC-derived NSPCs are thought to be a useful model to study HCMV neuropathogenesis and to analyze the mechanisms of HCMV-induced apoptosis in neural cells.

Keywords: Human cytomegalovirus, iPS cells, Neural stem/progenitor cells, Apoptosis, ER stress

* Correspondence: nakamura-hry@ncchd.go.jp
[1]Department of Infectious Diseases, National Research Institute for Child Health and Development, 2-10-1 Okura, Setagaya-ku, Tokyo 157-8535, Japan
Full list of author information is available at the end of the article

Background

Congenital cytomegalovirus (CMV) infection is a major cause of birth defects resulting mainly from primary CMV infection during pregnancy. At birth, approximately 5 to 10% of congenitally infected newborns are estimated to be symptomatic exhibiting multi-organ disorders including neurological defects such as mental retardation, sensorineural hearing loss, and microencephaly [1,2]. A latest study showed that if laboratory findings including those from magnetic resonance imaging (MRI) images of the brain are considered, up to 30% of congenitally infected newborns exhibit some abnormal signs [3]. Sixty to 90% of congenitally infected children who are symptomatic at birth, and 10 to 15% of those who are asymptomatic at birth develop one or more long-term sequelae. Although CMV infects a wide variety of cell types, infection of the nervous system gives most serious and long-lasting damages to the host.

As a part of understanding the HCMV neuropathogenesis, it is important to scrutinize the cellular response to CMV infection in neural cells. Some human neural cell lines can be infected with HCMV with different permissiveness to HCMV gene expression and replication [4-7]. A recent study has shown that neural progenitor cells isolated from developing human brain tissues are susceptible to CMV infection and undergo apoptosis following infection [8,9]. However, the amount of neural cells obtainable from human brain tissues is limited.

Pluripotent stem cells, including embryonic stem cells (ESCs) and induced pluripotent stem cells (iPSCs), are characterized by the ability to differentiate into tissues derived from any of the three embryonic germ layers. Recent advances in the method to induce efficient differentiation of either ESCs or iPSCs into specific cell lineages offer an opportunity to establish model systems for viral infections of various cell types, including neural cells. Furthermore, differentiated cells derived from pluripotent stem cells are obtainable in potentially unlimited amounts. Previous works revealed that while mouse ESCs are not susceptible to murine CMV (MCMV), NSPCs that are differentiated from them are susceptible and their proliferation and differentiation are suppressed by MCMV [10-13]. Experiments with human ESCs are, however, complicated with ethical problems.

In this study, to analyze the pathological effects of HCMV on neural cells, we prepared NSPCs from human iPSCs and examined whether NSPCs are susceptible to HCMV infection. The results indicated that NSPCs are susceptible to HCMV infection and undergo apoptosis caused by mitochondrial dysfunction and endoplasmic reticulum (ER) stress.

Methods

Cells and viruses

The human fetal lung fibroblast MRC5 was grown in Dulbecco's modified Eagle's medium (DMEM) supplemented with 10% fetal bovine serum (FBS; Invitrogen, Carlsbad, CA). The human foreskin fibroblast cell line hTERT-BJ1 immortalized with the human telomerase reverse transcriptase (Clontech, Palo Alto, CA) was grown in a medium consisting of 4 parts of DMEM and 1 part of medium 199 (Sigma) supplemented with 10% FBS, 1 mM sodium pyruvate (Sigma), and 2 mM glutamine (Invitrogen). HCMV laboratory strain Towne (ATCC VR-977) was propagated in hTERT-BJ1 cells. The human iPSC line MRC-iPS-25 that was established from MRC5 by retroviral vector-mediated transduction of the c-Myc, Oct-4, Klf4, and Sox2 genes [14,15] were cultured on mitomycin C-treated mouse embryonic fibroblasts (MEFs) in an iPSC medium consisting of Knockout DMEM/F12 (Invitrogen) supplemented with non-essential amino acids (0.1 mM, Invitrogen), glutamax I (1 mM, Invitrogen), 20% Knockout Serum Replacement (Invitrogen), β-mercaptoethanol (55 μM, Invitrogen) and basic fibroblast growth factor (10 ng/mL; Peprotech, Rocky Hill, NJ).

Induced differentiation on iPSCs into neural stem cells

MRC-iPSC-25 cells cultured under feeder-free conditions were induced to differentiate into neural stem/progenitor cells (NSPCs) by the method of dual inhibition of the SMAD signaling pathway described previously [16]. In brief, feeder-free iPSCs were treated with the mTeSR1 medium (StemCell Technologies, Vancouver, BC, Canada) containing Y27632 (Wako Pure Chemicals, Osaka, Japan) and maintained with a daily medium change for 4 days. Then the medium was replaced with iPSC medium supplemented with SB431542 (10 nM, Wako Pure Chemicals) and Noggin (500 ng/ml, Wako Pure Chemicals). This date was designated day 0. On day 2, culture medium was replaced with a medium consisting of 3 parts of iPSC medium and 1 part of N2 medium (Knockout DMEM/F12 containing 1× N2 supplement) supplemented with SB431542 (10 nM) and Noggin (500 ng/ml). On day 4, culture medium was replaced with a medium consisting of 1 part of iPSC medium and 1 part of N2 medium supplemented with SB431542 (10 nM) and Noggin (500 ng/ml). On day 6, cells were expanded in StemPro NSC SFM (Invitrogen). MRC-iPSC-25 cells cultured under feeder-free conditions and NSPC/iPSCs were infected with the Towne strain HCMV at a multiplicity of infection (MOI) of 1 plaque forming unit (PFU) per cell. To detect infectious virions produced from HCMV-infected NSPC/iPSCs, supernatant was collected and replaced with fresh medium every two days after infection. hTERT-BJ1 cells were inoculated with the supernatant and examined by IFA for expression of IE1/IE2.

Antibodies

Antibodies used were as follows: rabbit anti-Sox2, rabbit anti-Nanog, rabbit anti-Oct-4, rabbit anti-cleaved caspase-

3, rabbit anti-cleaved caspase-9, rabbit anti-phospho-eIF2α (Ser51), rabbit anti-phospho-PERK (Thr980), and rabbit anti-phospho-SAPK/JNK (Thr183/Tyr185)(Cell Signaling Technology, Beverly, MA); mouse anti-CMV IE1/IE2, rabbit anti-Musashi-1, and rabbit anti-cytochrome c (Millipore, Temecula, CA); rabbit anti-Nestin and mouse anti-α-tubulin (Sigma-Aldrich, St. Louis, MO); rabbit anti-Pax6 (Covance, Princeton, NJ), mouse anti-CMV gB (Abcam, Cambridge, MA); mouse anti-pp65 (Virusys Corporation, Sykesville, MD); rabbit anti-phosphorylated IRE1α (Pierce/Thermo Scientific, Rockford, IL); Alexa Fluor 488-conjugated goat anti-mouse IgG and Alexa Fluor 594-conjugated goat anti-rabbit IgG (Molecular Probes, Eugene, OR); horseradish peroxidase-conjugated donkey anti-rabbit IgG and horseradish peroxidase-conjugated sheep anti-mouse IgG (GE Healthcare, UK).

Immunofluorescence microscopy and immunoblot analysis

Cells were fixed with 4% parafolmaldehyde in PBS (Wako chemicals) at room temperature (RT) for 15 min. After fixation, cells were treated with 1.0% Triton X-100 in PBS for 15 min at RT and blocked with 10% goat serum in PBS for 30 min. Cells were incubated with the primary antibody at 4°C overnight, followed by washing in PBS and incubation with the corresponding secondary antibody at 37°C for 1 h. Nuclei were stained with DAPI. For the assessment of cell death, terminal deoxynucleotidyl transferase (TdT)-mediated dUTP nick-end labeling (TUNEL) assay was performed according to the manufacturer's instructions (Roche). Immunoblot analyses were performed as described previously [17].

Reverse transcriptase (RT)-PCR and real-time quantitative RT-PCR

Total RNA was isolated from mock- or HCMV-infected cells using TRIzol reagent (Invitrogen). Reverse transcription was performed on each RNA sample (5 μg) using SuperScript III First-Strand Synthesis System for RT-PCR (Invitrogen). Primer sequences are shown in Table 1. RT-PCR products were resolved by electrophoresis on 2% agarose gel and then visualized by ultraviolet illumination after ethidium bromide staining. Real-time quantitative RT-PCR was performed using TaqMan™ Universal Master Mix II with UNG (Applied Biosystems) on a StepOne Plus PCR System (Applied Biosystems). Amplifications were achieved in a final volume of 25 μl containing TaqMan probes labeled with FAM on the 5'-end and MGB on the 3'-end. The primers and probes for *UL136* were: forward primer, 5'-GGCCGTTGAACGGAGCTAT-3' and reverse primer, 5'-CCATTTCCACCGTGTCGAA-3', and TaqMan probe, 5'-FAM-TACTACGGCAGCGGCT-MGB-3'. The forward and reverse primers and reporter probes for HCMV *IE1*, *UL89*, and Human *G6PD* were described previously [18].

Table 1 List of primer sequences for RT-PCR

Gene	Forward primer	Reverse primer
IE1*	ATGGAGTCCTCTGCCAAGAG	ATTCTATGCCGCACCATGTCC
IE2*	ATGGAGTCCTCTGCCAAGAG	CTGAGACTTGTTCCTCAGGTCCTG
vIL-10*	ATGCTGTCGGTGATGGTCTCTTCC	CTTTCTCGAGTGCAGATACTCTTCG
UL36*	GACCTACGGGACACGCTGATG	TGTGGAAGTGGTCGCAGTGAC
UL38	GACTACGACCACGCATAGCA	GGGAACAGAGCGTTCCAATA
pp65	CGCAACCTGGTGCCCATGG	CGTTTGGGTTGCGCAGCGGG
Nanog*	GCTTGCCTTGCTTTGAAGCA	TTCTTGACCGGGACCTTGTC
Oct-4	GAGCAAAACCCGGAGGAGT	TTCTCTTTCGGGCCTGCAC
Sox1	GCGGAAAGCGTTTTCTTTG	TAATCTGACTTCTCCTCCC
Sox2	ATGCACCGCTACGACGTGA	CTTTTGCACCCCTCCCATTT
Pax6*	AACAGACACAGCCCTCACAAACA	CGGGAACTTGAACTGGAACTGAC
Nestin*	CAGCGTTGGAACAGAGGTTGG	TGGCACAGGTGTCTCAAGGGTAG
MAP2*	CCACCTGAGATTAAGGATCA	GGCTTACTTTGCTTCTCTGA
GFAP*	GTACCAGGACCTGCTCAAT	CAACTATCCTGCTTCTGCTC
OSP*	ACTGCTGCTGACTGTTCTTC	GTAGAAACGGTTTTCACCAA
XBP1*	CCTTGTAGTTGAGAACCAGG	GGGGCTTGGTATATATGTGG
CHOP*	TGGAAGCCTGGTATGAGGAC	TCACCATTCGGTCAATCAGA
β-actin*	ACCATGGATGATGATATCGC	TCATTGTAGAAGGTGTGGTG
GAPDH*	CCACCCATGGCAAATTCCATGGCA	TCTAGACGGCAGGTCAGGTCCACC

Asterisks (*) indicate that amplified fragments contain splicing junctions. Amplified fragments for UL38, pp65, Oct-4, Sox1, and Sox2 did not contain splicing junctions, and therefore control experiments without reverse transcriptase confirmed the RNA origin of the PCR products.

Results

Preparation of human iPSC-derived neural stem/progenitor cells

Figure 1A demonstrates that MRC-iPS-25 cells have a typical iPSC colony morphology. The expression of pluripotency markers of iPSCs such as Nanog and Oct-4 in MRC-iPS-25 cells was confirmed by indirect immunofluorescence assay (IFA) (Figure 1B). The HCMV-encoded proteins IE1/IE2 were not detected in MRC-iPS-25 cells following inoculation with the virus, indicating that MRC-iPS-25 cells are either not susceptible to HCMV infection or do not support expression of the IE genes (Figure 1B).

NSPC/iPSCs prepared by induced differentiation of MRC-iPS-25 cells proliferated in a monolayer and displayed a rounded, immature neural morphology (Figure 1A). IFA (Figure 1C) showed that NSPC/iPSCs expressed the NSC markers Nestin, Sox2, and Pax6, indicating that NSPC/iPSCs have the authentic NSPC phenotype.

In vitro HCMV infection of iPSC-derived NSPCs

To examine the susceptibility of NSPC/iPSCs to HCMV infection, these cells were inoculated in vitro with the HCMV Towne strain at an MOI of 1 PFU per cell (Figure 2A). On the second day post-infection (dpi), NSPC/iPSCs started to show morphological changes including increased cell volume and cell fusion, and the number of cells with these

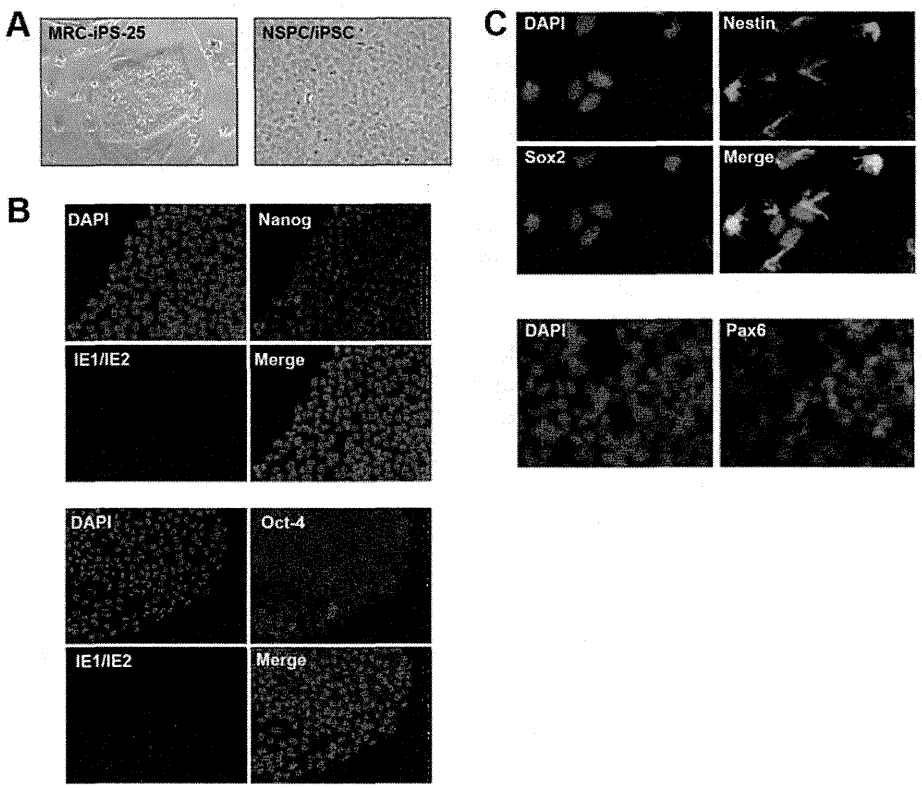

Figure 1 Differentiation of MRC-iPS-25 cells to neural stem/progenitor cells. (A) Phase-contrast images of MRC-iPS-25 cells cultured on a feeder layer of MEFs (left) and NSPC/iPSCs (right). **(B)** Immunofluorescence analysis of Towne-infected MRC-iPS-25 cells cultured under feeder-free conditions at 2 dpi stained with primary antibodies for pluripotent markers (Nanog or Oct-4) and HCMV IE1/IE2 proteins. Antigen proteins were detected with Alexa Fluor 488-conjugated goat anti-mouse IgG or Alexa Fluor 594-conjugated goat anti-rabbit IgG antibody. Nuclei were stained with DAPI. **(C)** Immunofluorescence analysis of NSPC markers Nestin, Sox2, and Pax6 in NSPC/iPSCs. NSPC/iPSCs were fixed and reacted with anti-Nestin (green), anti-Sox2 (red), and anti-Pax6 (red) antibodies, followed by detection with secondary antibodies. Immunofluorescence signals were obtained using a fluorescence microscope IX71. Representative results from three independent experiments are shown.

changes increased until 7 dpi (Figure 2A). To examine whether NSPC/iPSCs were capable of supporting HCMV gene expression, total RNA extracted from the infected NSPC/iPSCs was analyzed by RT-PCR. As shown in Figure 2B, mRNAs encoding IE1, IE2, vIL-10, and pp65 as well as those encoding HCMV anti-apoptotic proteins, such as UL36 and UL38, were detected. The kinetics of HCMV gene expression was analyzed by quantitative real-time RT-PCR (Figure 2C). IE1 mRNA was detected first on 1 dpi and increased steadily until 5 dpi. mRNAs for UL89 and UL136 were detected somewhat later and increased gradually until 7 dpi. The results showed the NSPC/iPSCs are susceptible to HCMV infection and allow the expression of several viral genes of both early and late functions.

Expression of HCMV genes in NSPC/iPSCs was evaluated at the protein level by immunoblot analysis on day 1, 2, 5, and 7 following HCMV infection. As shown in Figure 2D, the immediate-early protein IE1 was first detected at 1 dpi and its level increased until 5 dpi. Another immediate-early protein IE2 was detected a little later, becoming visible at 5 dpi. The expression of the HCMV lower matrix protein pp65 (ppUL83), already visible at 1 dpi, was markedly elevated at 5 and 7 dpi. The HCMV envelope glycoprotein B (gB; UL55) was detected at 5 to 7 dpi. Thus the expression of HCMV proteins of both immediate-early and late functions was demonstrated in NSPC/iPSCs.

We next examined the expression of cellular mRNAs encoding the pluripotency and neural differentiation markers (Figure 2E). Expression of the iPSC markers Nanog and Oct-4 remained at low levels following infection with HCMV, although that of Nanog tapered. While expression of the NSPC markers Sox2 and Pax6 were kept at high levels following HCMV infection, that of another NSPC marker Nestin was markedly suppressed at 7 dpi. In addition, expression of the neuronal marker microtubule-associated protein 2 (MAP2), the astrocyte marker glial fibrillary acidic protein (GFAP), and the oligodendrocyte marker oligodendrocyte-specific protein (OSP) was detected at low levels. Interestingly, Sox1, a marker specific to the neuroectodermal lineages [19], was markedly upregulated following infection with HCMV. Expression of the NSPC markers was evaluated

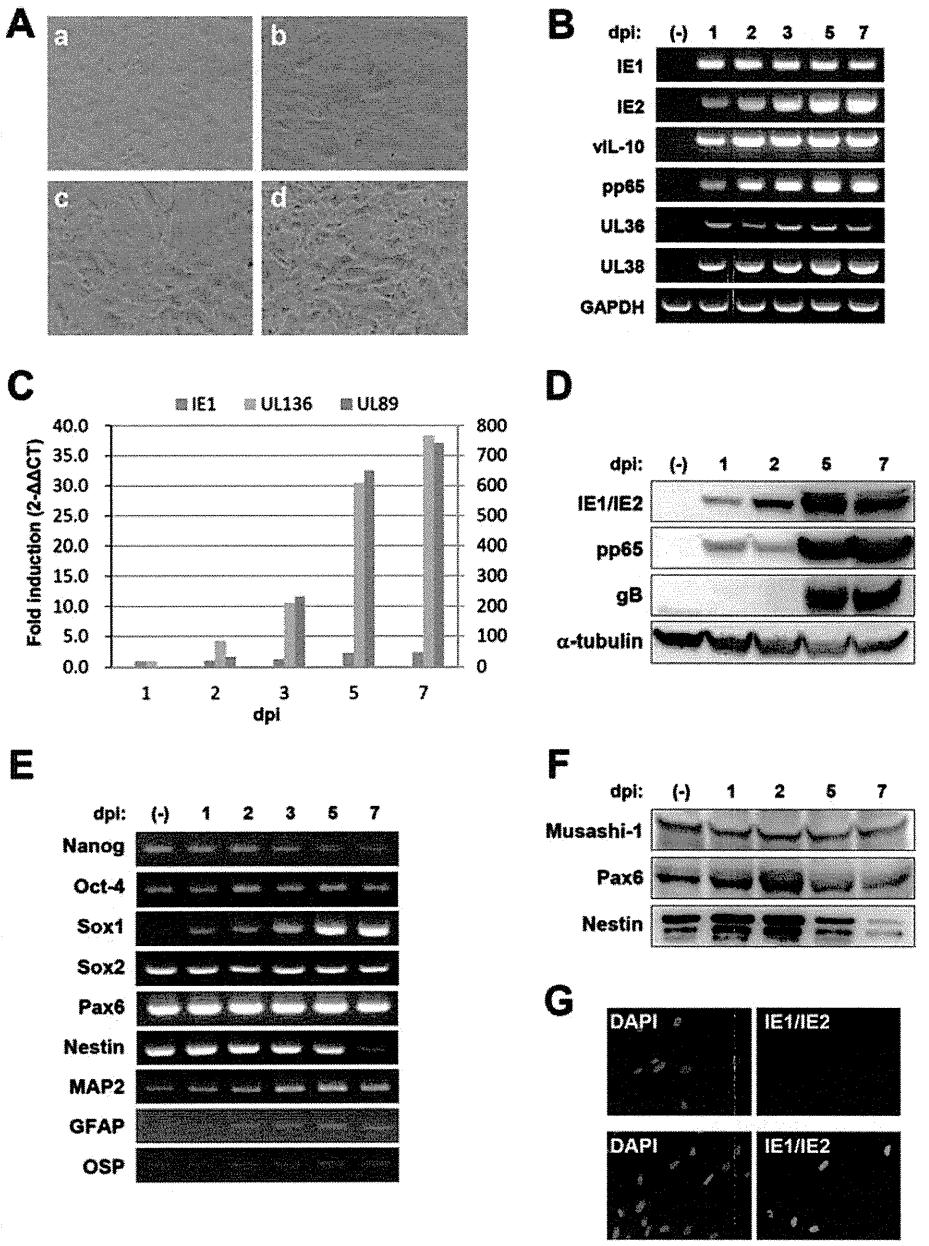

Figure 2 Analysis on the expression of viral and cellular gene products in NSPC/iPSCs. (A) Morphological changes of Towne-infected NSPC/iPSCs were observed under the inverted microscope before infection **(a)**, 2 dpi **(b)**, 5 dpi **(c)**, and 7 dpi **(d)**. **(B)** RT-PCR analysis of HCMV-encoding gene expression. Total RNAs isolated from NSPC/iPSCs harvested before (–) HCMV infection or at 1, 2, 3, 5, and 7 dpi with HCMV Towne strain were subjected to RT-PCR assays. GAPDH gene expression was assayed for the control. **(C)** The kinetics of mRNA expression for IE1, UL89, and UL136 in Towne-infected NSPC/iPSCs was examined by real-time quantitative RT-PCR assay. The mRNA expression was normalized to that of G6PDH gene. Real-time PCR data was analyzed by the 2-ΔΔCT method. The fold induction was calculated as the ratio of mRNA levels detected at each time point to that detected at 1 dpi. The y-axis represents fold induction of IE1 and UL136 mRNA (left y-axis) and UL89 mRNA (right y-axis). **(D)** Immunoblot analysis of HCMV protein expression in HCMV-infected NSPC/iPSCs. Whole-cell lysates of NSPC/iPSCs harvested before (–) HCMV infection or at 1, 2, 5, and 7 dpi with HCMV Towne strain were separated by SDS-PAGE and analyzed by immunoblotting with antibodies against IE1/IE2, pp65, gB, and α-tubulin. **(E)** RT-PCR analysis of pluripotency and neural differentiation marker gene expression in HCMV-infected NSPC/iPSCs. **(F)** Immunoblot analysis of neural differentiation marker protein expression in HCMV-infected NSPC/iPSCs. Whole-cell lysates of NSPC/iPSCs were analyzed by immunoblotting with antibodies against Musashi-1, Pax6, and Nestin. **(G)** hTERT-BJ1 cells inoculated with culture supernatant collected from mock-infected NSPC/iPSCs (upper panel) or Towne HCMV-infected NSPC/iPSCs (lower panel) at 8 dpi were subjected to immunofluorescence test with anti-IE1/IE2 antibody (green). Nuclei were stained with DAPI. Representative results from two independent experiments are shown.

also at the protein level by immunoblot analysis on 1, 2, 5, and 7 dpi (Figure 2F). In accordance with the results with RT-PCR, expression of Pax6 and Nestin was confirmed, and that of Nestin was found markedly decreased 7 dpi. Another NSPC marker Musashi-1 was also detected. To examine whether HCMV-infected NSPC/iPSCs produce infectious virions, culture supernatants collected from Towne HCMV-infected NSPC/iPSCs were inoculated to hTERT-BJ1 cells. Inoculated cells expressed IE1/IE2 indicating that infectious virions were produced from HCMV-infected NSPC/iPSCs (Figure 2G). The supernatant contained 30 PFU/mL of HCMV at 4, 6, 8 dpi, while no plaque forming virus was detected at 2 dpi.

HCMV infection induces apoptosis in iPSC-derived NSPCs

To examine whether HCMV infection in NSPC/iPSCs induces apoptotic responses, we performed the TUNEL assay combined with IFA using an antibody specific to HCMV gB. As shown in Figure 3A, NSPC/iPSCs expressing gB was positive for TUNEL staining and those without gB expression was consistently negative. We also performed IFA to analyze the activation status of caspases using antibodies specific to the activated forms of caspase-3 and caspase-9. The results show that the activated forms of caspase-3 and caspase-9 were specifically detected in more than 80% of HCMV-infected NSPC/iPSCs expressing IE1/IE2 proteins (Figure 3B and 3C), but not in mock-infected NSPC/iPSCs (Figure 3E). To see whether mitochondrial dysfunction is involved in the activation of caspase 9, intracellular distribution of cytochrome c was analyzed in HCMV-infected cells by IFA. As shown in Figure 3D and 3E, strong signals of cytochrome c were detected in the cytosol of cells expressing IE1/IE2 proteins, while only faint signals of cytochrome c were detected in cells not expressing IE1/IE2 proteins or in mock-infected cells. These results indicate that HCMV infection of NSPC/iPSCs activated apoptotic responses involving release of mitochondrial cytochrome c and serial activation of caspases.

Unfolded protein response in HCMV-infected NSPC/iPSCs

The unfolded protein response (UPR), induced by the accumulation of improperly folded proteins within the ER lumen (ER stress), is associated with multiple cellular responses such as neurodegeneration and apoptosis. ER stress sensor molecules, such as PKR-like eukaryotic initiation factor 2a kinase (PERK) and inositol-requiring enzyme 1 (IRE1), are activated on UPR and engage downstream signaling pathways. To examine whether the caspase-9 activation in HCMV-infected NSPC/iPSCs (Figure 3C) is associated with UPR, we analyzed phosphorylation status of IRE1α and its downstream target c-Jun NH2-terminal kinase (JNK) in immunofluorescence assays. Both IRE1α and JNK were specifically phosphorylated in HCMV-infected NSPC/iPSCs (Figure 4A and 4B), but not in mock-infected NSPC/iPSCs (Figure 4C). In concordance with the previous reports that activated IRE1α catalyzes the non-conventional splicing of the mRNA encoding X-box binding protein 1 (XBP1) [20,21], the spliced XBP1 mRNA increased gradually after HCMV infection in NSPC/iPSCs (Figure 4D). We also analyzed phosphorylation status of another sensor molecule PERK, an ER-associated serine/threonine protein kinase, and its downstream target the alpha subunit of eukaryotic initiation factor 2 (eIF2α). Phosphorylated forms of PERK and eIF2α were specifically detected in HCMV-infected NSPC/iPSCs (Figure 4E and 4F), but not in mock-infected NSPC/iPSCs (Figure 4G). The transcription factor activating transcription factor 4 (ATF4), that is preferentially translated on activation of PERK, induces the expression of C/EBP-homologous protein (CHOP/GADD153), a transcription factor with proapoptotic functions [22]. In accordance with these previous findings, the mRNA level of CHOP increased gradually after HCMV infection in NSPC/iPSCs (Figure 4H). These results suggest that UPR is involved in the activation of caspase cascade leading to apoptosis in HCMV-infected NSPC/iPSCs.

Discussion

Important findings in this study are as follows: i) NSPC/iPSCs derived from MRC-iPS-25 cells were susceptible to HCMV infection and allow the expression of viral gene products of both early and late functions and production of infectious virions. In contrast, MRC-iPS-25 cells before induction of differentiation was either resistant to HCMV or did not support the expression of HCMV immediate-early genes; ii) the HCMV-infected NSPCs undergo apoptosis; and iii) the mechanism of the apoptosis included cytochrome c release from mitochondria to cytosol and activation of UPR-related signaling pathways.

Neuropathogenesis of HCMV infection has been studied mainly with neural cells isolated from human brain. These studies demonstrated that HCMV can infect human neural precursor cells (NPCs) isolated from fetal brains and interfere with their differentiation. Luo et al. [23] showed that HCMV infection in primary NPCs reduced the expression of Nestin, suggesting that HCMV affects the differentiation potential of NPCs. Similar results were also obtained from experiments with mouse NSCs infected with MCMV [10,13,24]. Those previous findings obtained from experiments with primary cultures of brain-derived neural cells were thus mostly reproduced in our experiments using NSPC/iPSCs. In addition, similar to the results of Odeberg et al. [8] that used NPCs derived from human brain, we also demonstrated that HCMV infection induced apoptosis in NSPC/iPSCs obtained from iPSCs. It is thus supposed that neural cells differentiated from iPSCs are a useful

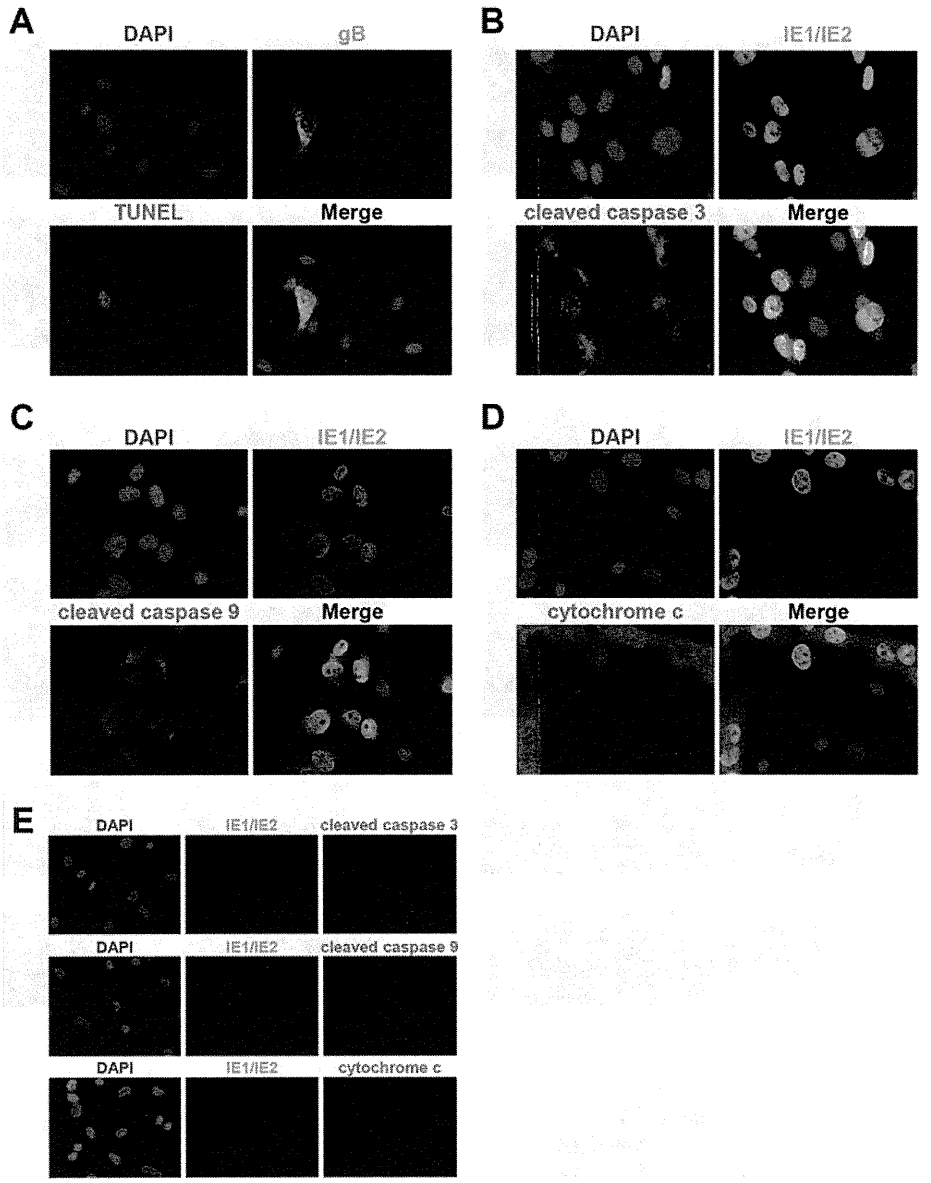

Figure 3 HCMV-induced apoptosis of NSPC/iPSCs. (A) Towne-infected NSPC/iPSCs at 6 dpi were subjected to TUNEL assay followed by immunofluorescence test with an anti-gB antibody. TUNEL-positive nuclei were stained in red. The anti-gB antibody was detected with Alexa Fluor 488-conjugated goat anti-mouse IgG antibody (green). Nuclei were stained with DAPI. **(B-D)** Towne-infected NSPC/iPSCs at 3 dpi were subjected to immunofluorescence test with anti-IE1/IE2 antibody in combination with anti-cleaved caspase 3 **(B)**, anti-cleaved caspase 9 **(C)**, or anti-cytochrome c **(D)** antibody. Alexa Fluor 488-conjugated goat anti-mouse IgG (green) or Alexa Fluor 594-conjugated goat anti-rabbit IgG antibody (red) was used as a secondary antibody. Nuclei were stained with DAPI. **(E)** Mock-infected NSPC/iPSCs were subjected to immunofluorescence test with anti-IE1/IE2 antibody in combination with anti-cleaved caspase 3 (upper panel), anti-cleaved caspase 9 (middle panel), or anti-cytochrome c (lower panel) antibody. Nuclei were stained with DAPI. Representative results from two independent experiments are shown.

model to investigate neural pathogenesis of HCMV. In the human brain, NSCs are predominantly found in the subventricular region where CMV infections preferentially occur [25,26]. Analysis on the effects of HCMV infection on NSPCs can be therefore particularly relevant.

In the regulation of cellular apoptotic responses, mitochondrial dysfunction and ER stress are involved in the activation of the initiator caspase caspase-9 that functions as a trigger of cascade protease reactions leading to cell death. The finding of cytochrome c release from mitochondria to cytoplasm in HCMV-infected NSPC/iPSCs indicates that mitochondrial dysfunction is involved in the activation of caspase-9 in these cells. In addition, the demonstration of phosphorylated forms of proteins involved in UPR, including PERK, JNK, IRE1α, eIF2α, as well as that of unconventional splicing of

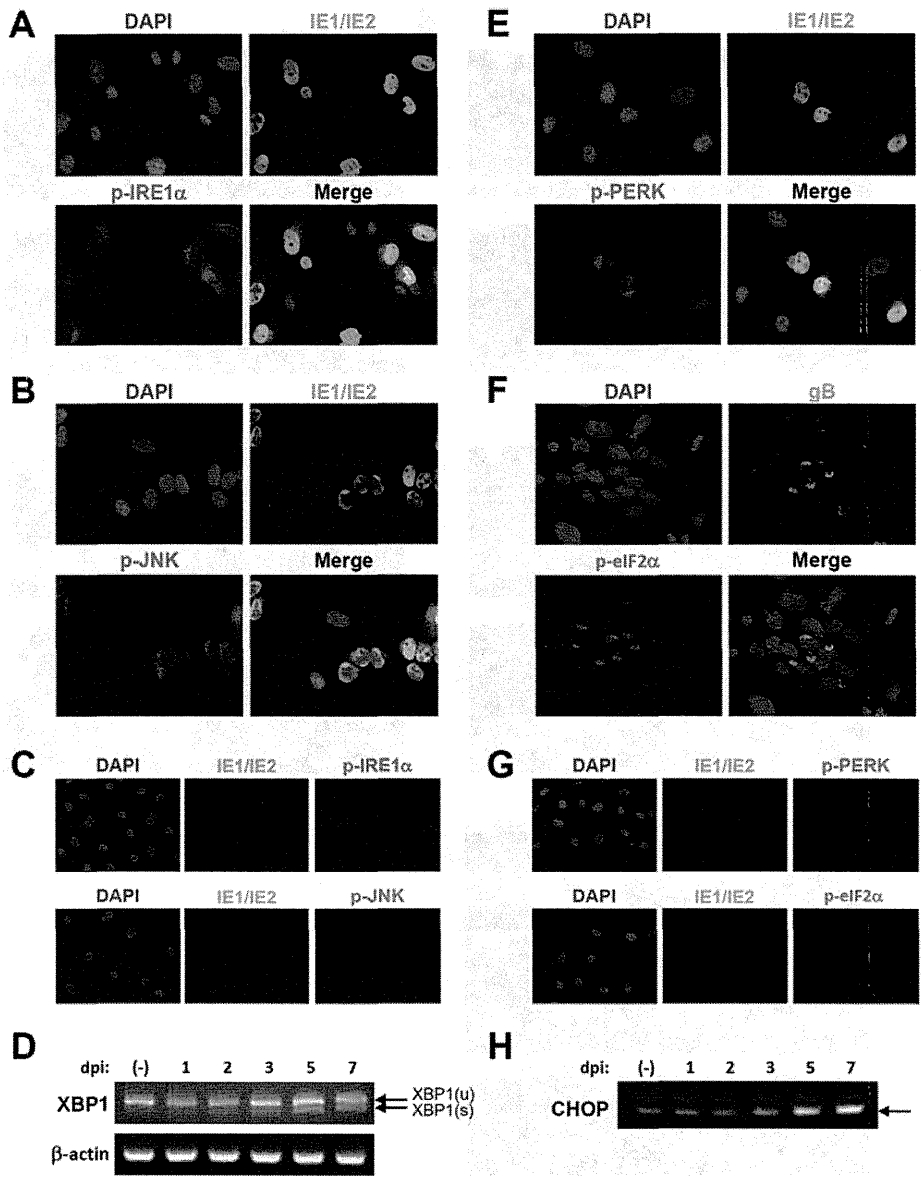

Figure 4 HCMV-induced UPR in NSPC/iPSCs. (A and B) Towne-infected NSPC/iPSCs at 3 dpi were subjected to immunofluorescence test with anti-IE1/IE2 antibody in combination with anti-phosphorylated IRE1α **(A)** or anti-phosphorylated JNK **(B)** antibody. Nuclei were stained with DAPI. **(C)** Mock-infected NSPC/iPSCs were subjected to immunofluorescence test with anti-IE1/IE2 antibody in combination with anti-phosphorylated IRE1α (upper panel) or anti-phosphorylated JNK (lower panel) antibody. Nuclei were stained with DAPI. **(D)** Detection of XBP1 (u, unspliced) and XBP1 (s, spliced) mRNAs in HCMV-infected NSPC/iPSCs. Total RNAs isolated from NSPC/iPSCs harvested before (–) HCMV infection or at 1, 2, 3, 5, and 7 dpi with HCMV Towne strain were subjected to RT-PCR assays. Amplified DNA fragments were separated in a 2% agarose gel and then photographed. Beta-actin gene expression was assayed for the control. **(E and F)** Towne-infected NSPC/iPSCs at 3 dpi were subjected to immunofluorescence test with anti-IE1/IE2 antibody in combination with anti-phosphorylated PERK **(E)** or anti-gB antibody in combination with anti-phosphorylated eIF2α **(F)** antibody. **(G)** Mock-infected NSPC/iPSCs were subjected to immunofluorescence test with anti-IE1/IE2 antibody in combination with anti-phosphorylated PERK (upper panel) or anti-phosphorylated eIF2α (lower panel) antibody. Nuclei were stained with DAPI. **(H)** Expression of CHOP mRNA in HCMV-infected NSPC/iPSCs. Total RNAs isolated from NSPC/iPSCs harvested before (–) HCMV infection or at 1, 2, 3, 5, and 7 dpi with HCMV Towne strain were subjected to RT-PCR assays. Representative results from three independent experiments are shown.

XBP1 mRNA and up-regulation of CHOP, indicate that ER stress also plays a role in HCMV-induced apoptosis of NSPC/iPSCs. These results are in accordance with the work reported by Isler et al. [27] who demonstrated that HCMV-induced UPR in human foreskin fibroblasts. HCMV is known to encode anti-apoptotic proteins such as viral inhibitor of caspase-8-induced apoptosis (vICA) encoded by UL36 [28], and pUL38 which protects against ER stress-induced cell death by modulating the UPR pathway [29]. Our RT-PCR analysis demonstrated

that such viral anti-apoptotic genes were expressed at transcription level in NSPC/iPSCs following HCMV infection (Figure 2B). Although these viral anti-apoptotic proteins did not block apoptosis of NSPC/iPSCs, they might have contributed for efficient viral replication by delaying apoptosis.

iPSCs are expected to be an innovative tool for not only regenerative medicine but also for the elucidation of pathogenesis of various diseases. Recent studies have shown that human iPSCs can be used also for modeling viral infection. Hepatocyte-like cells derived from human iPSCs were shown to be susceptible to hepatitis virus C infection and supported its replication [30,31]. Sensory neurons derived from human iPSCs were reported to be susceptible to infection with both varicella-zoster virus and herpes simplex virus [32]. While the present work was in progress, D'Aiuto and others reported on the preparation of an iPSC-derived model of HCMV infection in neural precursor cells [33]. Whereas our data described in the present study is largely consistent with their results, we further analyzed the mechanisms of apoptosis induction and elucidated the involvement of mitochondrial dysfunction and ER stress.

In conclusion, human NSPCs derived from iPSCs can be a useful model to study HCMV neuropathogenesis associated with congenital HCMV infection. They can be particularly valuable in analyzing the mechanisms of HCMV-induced apoptosis in neural cells.

Abbreviations

HCMV: Human cytomegalovirus; iPSC: Induced pluripotent stem cell; ESC: Embryonic stem cell; NSPC: Neural stem/progenitor cell; TUNEL: Terminal deoxynucleotidyl transferase-mediated dUTP nick-end labeling; UPR: Unfolded protein response; ER: Endoplasmic reticulum; PERK: PKR-like eukaryotic initiation factor 2a kinase; JNK: c-Jun NH2-terminal kinase; IRE1: Inositol-requiring enzyme 1; eIF2α: Alpha subunit of eukaryotic initiation factor 2; CHOP: C/EBP-homologous protein; XBP1: X-box binding protein 1; IFA: Indirect immunofluorescence assay; Dpi: Days post-infection; MAP2: Microtubule-associated protein 2; GFAP: Glial fibrillary acidic protein; OSP: Oligodendrocyte-specific protein; ATF4: Activating transcription factor 4; MOI: Multiplicity of infection.

Competing interests

The authors declare that they have no competing interests.

Authors' contributions

HN, HL, KM, and HA performed the experimental studies, and KI helped to analyze the data. KM, MT, HA, YM, HO, NK, and AU participated in the characterization of iPSCs and their derivatives. HN, HL, and SF wrote the manuscript. NI revised the manuscript. All authors read and approved the final manuscript.

Acknowledgments

We especially thank M. Katata for excellent technical assistance. This work was partly supported by Grants-in-Aid for Scientific Research from the Ministry of Education, Culture, Sports, Science and Technology of Japan (24591616), the Ministry of Health, Labour and Welfare of Japan (H23-Jisedai-Ippan-001), and the Grants of National Center for Child Health and Development (22A-9 and 24–17).

Author details

[1]Department of Infectious Diseases, National Research Institute for Child Health and Development, 2-10-1 Okura, Setagaya-ku, Tokyo 157-8535, Japan. [2]Department of Reproductive Biology, Center for Regenerative Medicine, National Research Institute for Child Health and Development, 2-10-1 Okura, Setagaya-ku, Tokyo 157-8535, Japan. [3]Department of Pediatric Hematology and Oncology Research, National Research Institute for Child Health and Development, 2-10-1 Okura, Setagaya-ku, Tokyo 157-8535, Japan. [4]Department of Virology I, National Institute of Infectious Diseases, 1-23-1 Toyama, Shinjuku-ku, Tokyo 162-8640, Japan.

Received: 17 April 2013 Accepted: 15 October 2013
Published: 21 October 2013

References

1. Cheeran MC, Lokensgard JR, Schleiss MR: **Neuropathogenesis of congenital cytomegalovirus infection: disease mechanisms and prospects for intervention.** *Clin Microbiol Rev* 2009, **22**(1):99–126. Table of Contents.
2. Revello MG, Gerna G: **Diagnosis and management of human cytomegalovirus infection in the mother, fetus, and newborn infant.** *Clin Microbiol Rev* 2002, **15**(4):680–715.
3. Koyano S, Inoue N, Oka A, Moriuchi H, Asano K, Ito Y, Yamada H, Yoshikawa T, Suzutani T: **Screening for congenital cytomegalovirus infection using newborn urine samples collected on filter paper: feasibility and outcomes from a multicentre study.** *BMJ Open* 2011, **1**(1):e000118.
4. Cinatl J Jr, Vogel JU, Cinatl J, Weber B, Rabenau H, Novak M, Kornhuber B, Doerr HW: **Long-term productive human cytomegalovirus infection of a human neuroblastoma cell line.** *Int J Cancer* 1996, **65**(1):90–96.
5. Cinatl J Jr, Cinatl J, Vogel JU, Kotchetkov R, Driever PH, Kabickova H, Kornhuber B, Schwabe D, Doerr HW: **Persistent human cytomegalovirus infection induces drug resistance and alteration of programmed cell death in human neuroblastoma cells.** *Cancer Res* 1998, **58**(2):367–372.
6. Luo MH, Fortunato EA: **Long-term infection and shedding of human cytomegalovirus in T98G glioblastoma cells.** *J Virol* 2007, **81**(19):10424–10436.
7. Ogura T, Tanaka J, Kamiya S, Sato H, Ogura H, Hatano M: **Human cytomegalovirus persistent infection in a human central nervous system cell line: production of a variant virus with different growth characteristics.** *J Gen Virol* 1986, **67**(Pt 12):2605–2616.
8. Odeberg J, Wolmer N, Falci S, Westgren M, Seiger A, Soderberg-Naucler C: **Human cytomegalovirus inhibits neuronal differentiation and induces apoptosis in human neural precursor cells.** *J Virol* 2006, **80**(18):8929–8939.
9. Odeberg J, Wolmer N, Falci S, Westgren M, Sundtrom E, Seiger A, Soderberg-Naucler C: **Late human cytomegalovirus (HCMV) proteins inhibit differentiation of human neural precursor cells into astrocytes.** *J Neurosci Res* 2007, **85**(3):583–593.
10. Cheeran MC, Jiang Z, Hu S, Ni HT, Palmquist JM, Lokensgard JR: **Cytomegalovirus infection and interferon-gamma modulate major histocompatibility complex class I expression on neural stem cells.** *J Neurovirol* 2008, **14**(5):437–447.
11. Matsukage S, Kosugi I, Kawasaki H, Miura K, Kitani H, Tsutsui Y: **Mouse embryonic stem cells are not susceptible to cytomegalovirus but acquire susceptibility during differentiation.** *Birth Defects Res A Clin Mol Teratol* 2006, **76**(2):115–125.
12. Li RY, Tsutsui Y: **Growth retardation and microcephaly induced in mice by placental infection with murine cytomegalovirus.** *Teratology* 2000, **62**(2):79–85.
13. Kosugi I, Shinmura Y, Kawasaki H, Arai Y, Li RY, Baba S, Tsutsui Y: **Cytomegalovirus infection of the central nervous system stem cells from mouse embryo: a model for developmental brain disorders induced by cytomegalovirus.** *Lab Invest* 2000, **80**(9):1373–1383.
14. Nishino K, Toyoda M, Yamazaki-Inoue M, Fukawatase Y, Chikazawa E, Sakaguchi H, Akutsu H, Umezawa A: **DNA methylation dynamics in human induced pluripotent stem cells over time.** *PLoS Genet* 2011, **7**(5):e1002085.
15. Makino H, Toyoda M, Matsumoto K, Saito H, Nishino K, Fukawatase Y, Machida M, Akutsu H, Uyama T, Miyagawa Y, *et al*: **Mesenchymal to embryonic incomplete transition of human cells by chimeric OCT4/3 (POU5F1) with physiological co-activator EWS.** *Exp Cell Res* 2009, **315**(16):2727–2740.
16. Chambers SM, Fasano CA, Papapetrou EP, Tomishima M, Sadelain M, Studer L: **Highly efficient neural conversion of human ES and iPS cells by dual inhibition of SMAD signaling.** *Nat Biotechnol* 2009, **27**(3):275–280.

17. Nakamura H, Lu M, Gwack Y, Souvlis J, Zeichner SL, Jung JU: **Global changes in Kaposi's sarcoma-associated virus gene expression patterns following expression of a tetracycline-inducible Rta transactivator.** *J Virol* 2003, **77**(7):4205–4220.
18. White EA, Clark CL, Sanchez V, Spector DH: **Small internal deletions in the human cytomegalovirus IE2 gene result in nonviable recombinant viruses with differential defects in viral gene expression.** *J Virol* 2004, **78**(4):1817–1830.
19. Pevny LH, Sockanathan S, Placzek M, Lovell-Badge R: **A role for SOX1 in neural determination.** *Development* 1998, **125**(10):1967–1978.
20. Calfon M, Zeng H, Urano F, Till JH, Hubbard SR, Harding HP, Clark SG, Ron D: **IRE1 couples endoplasmic reticulum load to secretory capacity by processing the XBP-1 mRNA.** *Nature* 2002, **415**(6867):92–96.
21. Sidrauski C, Walter P: **The transmembrane kinase Ire1p is a site-specific endonuclease that initiates mRNA splicing in the unfolded protein response.** *Cell* 1997, **90**(6):1031–1039.
22. Scheuner D, Song B, McEwen E, Liu C, Laybutt R, Gillespie P, Saunders T, Bonner-Weir S, Kaufman RJ: **Translational control is required for the unfolded protein response and in vivo glucose homeostasis.** *Mol Cell* 2001, **7**(6):1165–1176.
23. Luo MH, Hannemann H, Kulkarni AS, Schwartz PH, O'Dowd JM, Fortunato EA: **Human cytomegalovirus infection causes premature and abnormal differentiation of human neural progenitor cells.** *J Virol* 2010, **84**(7):3528–3541.
24. Mutnal MB, Cheeran MC, Hu S, Lokensgard JR: **Murine cytomegalovirus infection of neural stem cells alters neurogenesis in the developing brain.** *PLoS One* 2011, **6**(1):e16211.
25. Grassi MP, Clerici F, Perin C, D'Arminio Monforte A, Vago L, Borella M, Boldorini R, Mangoni A: **Microglial nodular encephalitis and ventriculoencephalitis due to cytomegalovirus infection in patients with AIDS: two distinct clinical patterns.** *Clin Infect Dis* 1998, **27**(3):504–508.
26. Perlman JM, Argyle C: **Lethal cytomegalovirus infection in preterm infants: clinical, radiological, and neuropathological findings.** *Ann Neurol* 1992, **31**(1):64–68.
27. Isler JA, Skalet AH, Alwine JC: **Human cytomegalovirus infection activates and regulates the unfolded protein response.** *J Virol* 2005, **79**(11):6890–6899.
28. Skaletskaya A, Bartle LM, Chittenden T, McCormick AL, Mocarski ES, Goldmacher VS: **A cytomegalovirus-encoded inhibitor of apoptosis that suppresses caspase-8 activation.** *Proc Natl Acad Sci U S A* 2001, **98**(14):7829–7834.
29. Terhune S, Torigoi E, Moorman N, Silva M, Qian Z, Shenk T, Yu D: **Human cytomegalovirus UL38 protein blocks apoptosis.** *J Virol* 2007, **81**(7):3109–3123.
30. Schwartz RE, Trehan K, Andrus L, Sheahan TP, Ploss A, Duncan SA, Rice CM, Bhatia SN: **Modeling hepatitis C virus infection using human induced pluripotent stem cells.** *Proc Natl Acad Sci U S A* 2012, **109**(7):2544–2548.
31. Wu X, Robotham JM, Lee E, Dalton S, Kneteman NM, Gilbert DM, Tang H: **Productive hepatitis C virus infection of stem cell-derived hepatocytes reveals a critical transition to viral permissiveness during differentiation.** *PLoS Pathog* 2012, **8**(4):e1002617.
32. Lee KS, Zhou W, Scott-McKean JJ, Emmerling KL, Cai GY, Krah DL, Costa AC, Freed CR, Levin MJ: **Human sensory neurons derived from induced pluripotent stem cells support varicella-zoster virus infection.** *PLoS One* 2012, **7**(12):e53010.
33. D'Aiuto L, Di Maio R, Heath B, Raimondi G, Milosevic J, Watson AM, Bamne M, Parks WT, Yang L, Lin B, *et al*: **Human induced pluripotent stem cell-derived models to investigate human cytomegalovirus infection in neural cells.** *PLoS One* 2012, **7**(11):e49700.

doi:10.1186/2042-4280-4-2
Cite this article as: Nakamura *et al.*: Human cytomegalovirus induces apoptosis in neural stem/progenitor cells derived from induced pluripotent stem cells by generating mitochondrial dysfunction and endoplasmic reticulum stress. *Herpesviridae* 2013 **4**:2.

Biochemical and Biophysical Research Communications 438 (2013) 753–759

Contents lists available at ScienceDirect

Biochemical and Biophysical Research Communications

journal homepage: www.elsevier.com/locate/ybbrc

N-Cadherin is a prospective cell surface marker of human mesenchymal stem cells that have high ability for cardiomyocyte differentiation

Hisako Ishimine [a,b], Norio Yamakawa [a], Mari Sasao [c], Mika Tadokoro [c], Daisuke Kami [d], Shinji Komazaki [e], Makoto Tokuhara [f], Hitomi Takada [a], Yoshimasa Ito [a], Shinichiro Kuno [g], Kotaro Yoshimura [g], Akihiro Umezawa [d], Hajime Ohgushi [c], Makoto Asashima [a,h,i,*], Akira Kurisaki [a,b,*]

[a] Research Center for Stem Cell Engineering, National Institute of Advanced Industrial Science and Technology (AIST), Tsukuba, Ibaraki, Japan
[b] Graduate School of Life and Environmental Sciences, The University of Tsukuba, Tsukuba, Ibaraki, Japan
[c] Health Research Institute, National Institute of Advanced Industrial Science and Technology (AIST), Amagasaki, Hyogo, Japan
[d] Department of Reproductive Biology and Pathology, National Research Institute for Child Health and Development, Setagaya, Tokyo, Japan
[e] Department of Anatomy, Saitama Medical School, Iruma, Saitama, Japan
[f] Department of Surgery, Research Institute National Center for Global Health and Medicine, Shinjuku, Tokyo, Japan
[g] Department of Plastic Surgery, University of Tokyo School of Medicine, Bunkyo, Tokyo, Japan
[h] Department of Life Sciences (Biology), Graduate School of Arts and Sciences, The University of Tokyo, Meguro, Tokyo, Japan
[i] Life Science Center of TARA, The University of Tsukuba, Tsukuba, Ibaraki, Japan

ARTICLE INFO

Article history:
Received 13 July 2013
Available online 27 July 2013

Keywords:
N-cadherin
Flk-1
c-Kit
Cardiomyocyte
Mesenchymal stem cells

ABSTRACT

Mesenchymal stem cells (MSCs) are among the most promising sources of stem cells for regenerative medicine. However, the range of their differentiation ability is very limited. In this study, we explored prospective cell surface markers of human MSCs that readily differentiate into cardiomyocytes. When the cardiomyogenic differentiation potential and the expression of cell surface markers involved in heart development were analyzed using various immortalized human MSC lines, the MSCs with high expression of N-cadherin showed a higher probability of differentiation into beating cardiomyocytes. The differentiated cardiomyocytes expressed terminally differentiated cardiomyocyte-specific markers such as α-actinin, cardiac troponin T, and connexin-43. A similar correlation was observed with primary human MSCs derived from bone marrow and adipose tissue. Moreover, N-cadherin-positive MSCs isolated with N-cadherin antibody-conjugated magnetic beads showed an apparently higher ability to differentiate into cardiomyocytes than the N-cadherin-negative population. Quantitative polymerase chain reaction analyses demonstrated that the N-cadherin-positive population expressed significantly elevated levels of cardiomyogenic progenitor-specific transcription factors, including *Nkx2.5*, *Hand1*, and *GATA4* mRNAs. Our results suggest that N-cadherin is a novel prospective cell surface marker of human MSCs that show a better ability for cardiomyocyte differentiation.

1. Introduction

Stem cell therapy is expected to be an alternative regenerative medicine. In addition to embryonic stem (ES) cells and induced pluripotent stem (iPS) cells, mesenchymal stem cells (MSCs) have been shown to differentiate into various cell types including osteoblasts, chondrocytes, adipocytes, neurons, skeletal muscle fibers, and cardiomyocytes *in vitro*. However, the differentiation ability of MSCs toward cardiomyocytes is still limited [1–3]. To overcome this problem, cell surface markers specific for cardiomyogenic progenitor cells could be used to enrich better population for regenerative medicine of heart failure.

Flk-1, a vascular endothelial growth factor receptor (VEGFR2), has been reported to be a prospective cell surface marker of cardiomyocyte progenitor cells during heart development [4,5]. Flk-1 is expressed in the progenitors of multiple mesodermal lineages, including cardiac, endothelial, and vascular smooth muscle cells [5]. c-Kit (CD117) is a transmembrane tyrosine kinase receptor for Stem cell factor, and used as a cell surface marker for hematopoietic progenitors, melanocytes, mast cells, and spermatogonial stem cells. Recent research has suggested that c-Kit could be a putative cell surface marker for cardiomyogenic progenitor cells in the neonatal heart [6].

A Ca^{2+}-dependent cell–cell adhesion molecule, N-cadherin, is also expressed on cardiomyocyte progenitor cells during mouse development. N-Cadherin expression is observed in the precardiac

* Corresponding authors. Address: Research Center for Stem Cell Engineering, National Institute of Advanced Industrial Science and Technology (AIST), Tsukuba AIST Central 4-1-3105, Higashi 1-1-1, Tsukuba, Ibaraki, 305-8562, Japan. Fax: +81 29 861 2987.
E-mail addresses: asashi@bio.c.u-tokyo.ac.jp (M. Asashima), akikuri@hotmail.com (A. Kurisaki).

0006-291X/$ - see front matter © 2013 Elsevier Inc. All rights reserved.
http://dx.doi.org/10.1016/j.bbrc.2013.07.081

mesoderm at E8.5 in mice and continues to be expressed in the whole heart during development. N-Cadherin-knockout mice died by E10 because of defects in the primitive heart. Although myocardial tissue was initially formed in the knockout mouse embryos, the myocytes were subsequently dissociated, and the heart tube failed to develop [7].

In this study, we explored cell surface markers of human MSCs that have a high ability to differentiate into cardiomyocytes. We show that N-cadherin is a prospective cell surface marker of MSCs with high cardiomyogenic potential.

2. Materials and methods

2.1. Cell culture

Human MSC cell lines, UE7T-13, UE6E7T-11, UBE6T-15, UE6E7T-12, UE7T-9, and UE6E7T-2, were obtained from the JCRB Cell Bank (Osaka, Japan). They were immortalized by retrovirus gene transfer of a combination of *bmi-1*, *E6*, *E7*, and/or *hTERT* genes to human bone marrow stromal cells harvested from a 91-year-old woman [8,10]. The EPC-214 cell line was similarly immortalized at the National Research Institute for Child Health and Development (NRICHD), Japan [9]. These cell lines were maintained in DMEM high glucose (Wako) supplemented with 10% fetal calf serum (FCS; Roche). As for the primary MSCs, ANP0425 and 0607NC, were obtained from Dr. Ohgushi (National Institute of Advanced Industrial Science and Technology, Japan). MSC-R36_2 cells, MSC-R36_3 cells, and Yub623 cells were obtained from the RIKEN BRC Cell Bank (Ibaraki, Japan). Primary MSCs derived from adipose tissue (ASCs), including 09-036 (36) cells, 10-008 (8) cells, 05-055 (55) cells, and 05-076 (76) cells, were prepared at the University of Tokyo, School of Medicine Tokyo, Japan. KN-SC (KN) cells, MY-SC (MY) cells, and NN-SC (NN) cells were prepared at the Research Institute National Center for Global Health and Medicine (NCGM), Japan. Other ASCs were purchased from Invitrogen. For the ASCs, all samples except KN-SC were obtained from women aged 22–45 years (KN-SC was derived from a 41-year-old man). All of these primary cells were maintained in MesenPRO RS Basal Medium supplemented with MesenPRO RS Growth Supplement (GIBCO). Cells were maintained in a humidified incubator at 37 °C with an atmosphere of 5% CO_2. All the experiments using human materials were approved by the Human Ethics Committee at AIST, NRICHD, NCGM, and the University of Tokyo. Human umbilical vein endothelial cells (HUVEC) were cultured in RPMI-1640 supplemented with EGM-2 SingleQuots (LONZA) and penicillin/streptomycin (Wako). TF-1 cells were cultured in RPMI-1640 supplemented with 10% FBS, 2 ng/mL rhGM-CSF, and penicillin/streptomycin (Wako).

2.2. Preparation of mouse fetal cardiomyocytes

The fetal hearts of E16.5 ICR mice were cut into small pieces and washed with phosphate-buffered saline (PBS). They were incubated with 0.15% trypsin and 0.012% EDTA in PBS at 37 °C for 10 min under gentle stirring. The supernatant containing the dissociated cardiomyocytes was mixed with DMEM supplemented with 10% FCS, and centrifuged at 1000 rpm for 5 min. The pellet was then re-suspended in 10 mL of DMEM with 10% FCS and incubated on a glass dish for 1 h to remove fibroblasts. The floating cardiomyocytes were collected and re-plated at $5 \times 10^5/cm^2$ on gelatin-coated glass bottom dishes (Asahi Techno Glass). All the experiments using animals were approved by the Animal Experiment Committee at AIST.

2.3. Immunoblotting analysis

Human MSC cell lines were homogenized in a lysis buffer containing 20 mM Tris–HCl (pH 7.4), 300 mM NaCl, 0.5 mM EDTA, 1% NP-40, and a complete protease inhibitor cocktail (Roche). After centrifugation at 13,000 rpm for 10 min at 4 °C, equal protein amounts were separated by SDS–PAGE (5–20%). The blots were incubated with antibodies against N-cadherin (1:200; C3865, Sigma), Flk-1 (1:100, 10347; IBL), c-Kit (1:200, AF332; R&D Systems), Integrin-α4 (1:200; sc-14008, Santa Cruz), VCAM-1 (1:200; sc-8304, Santa Cruz), PDGFRα (1:200; 323503, BioLegend), Nkx2.5 (1:200; sc-14033, Santa Cruz), GATA4 (1:200; sc-9053, Santa Cruz), or β-tubulin (1:1000, RB-9249; NeoMarkers). Proteins were detected with an enhanced chemiluminescence (ECL) reagent (Super-Signal West Femto Maximum Sensitivity Substrate, Pierce) using an LAS-3000 Image Analyzer (Fuji Film).

2.4. Flow cytometry analysis

All MSCs were harvested with cell dissociation buffer (GIBCO) and blocked with normal sheep IgG on ice for 1 h. Cells were incubated with biotinylated anti-N-cadherin antibody (1:100, BAF1388; R&D System), anti-Flk-1 antibody (1:100, 10347; IBL), and APC-conjugated anti-c-Kit antibody (1:100, 550412; Becton Dickinson) on ice for 1 h. The N-cadherin antibody was fluorescently labeled using Allophycocyanin-Alexa Fluor 750 streptavidin (Molecular Probes). The Flk-1 antibody was fluorescently labeled with the Alexa Fluor 488-conjugated secondary antibody (Molecular Probes). Cells were resuspended in buffer with propidium iodide (Sigma). Analysis was performed with a FACS Aria (Becton Dickinson) and FlowJo software (TOMY Digital Biology) with propidium iodide-negative population. The data were obtained from at least two independent experiments.

3. Results

MSCs are a mixture of primary adherent cells derived from the stroma of adult tissues. The multipotency of MSCs rapidly decreases as the passage number increases. Therefore, it is not easy to obtain reproducible data from these heterogeneous primary cells. To overcome these problems, we took advantage of immortalized human MSC clones with *bmi-1*, *TERT*, *E6*, and/or *E7*, which retain their multipotent differentiation ability over a long time when cultured *in vitro* [8].

Cardiac differentiation of human MSCs was performed by co-culturing with mouse fetal cardiomyocytes, which is a well-established method to differentiate MSCs into electro-physiologically validated cardiomyocytes [9,10]. Human MSC cell lines were labeled with a GFP-expressing lentivirus and then cultured on a cardiomyocyte feeder cells prepared from mouse embryonic heart tissue (Fig. S1A). On day 7, human MSC lines such as EPC-214 and UE7T-13 differentiated into cardiomyocytes. Around 5% of these GFP-labeled MSCs differentiated into beating cardiomyocytes (Fig. 1A). GFP-positive, differentiated cardiomyocytes showed autonomously periodical contractions (Fig. S1B). Significant number of GFP-positive human MSCs expressed cardiomyocyte-specific terminal differentiation markers (Fig. S1C, left and middle, Fig. S1D, left, and a confocal image Fig. S1E). On the other hand, some cell lines did not differentiate into beating cardiomyocytes under identical conditions (UE7T-9, UE6E7T-2) (Fig. S1C right and Fig. S1D right).

Next, the efficiency of human MSCs differentiation into spontaneously beating cardiomyocytes was quantified by counting the number of GFP-positive and spontaneously beating cardiomyocytes with a fluorescence microscope on day 7 (Fig. 1A). The

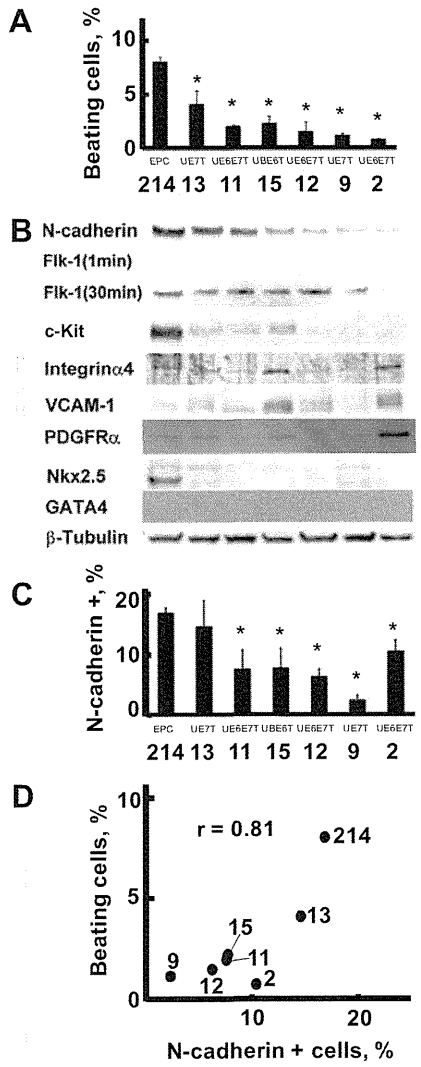

Fig. 1. Correlation between cardiomyogenic differentiation efficiency and cell surface protein marker expression in human MSC cell lines. (A) Autonomously beating cardiomyocytes differentiated from GFP-labeled human MSC lines, EPC-214, UE7T-13, UE6E7T-11, UBE6T-15, UE6E7T-12, UE7T-9, and UE6E7T-2, were counted under a fluorescence microscope. (B) The expression of cell surface proteins and transcription factors related to cardiovascular development were analyzed by immunoblotting of whole cell lysates. (C) Flow cytometric analysis of cell surface expression of N-cadherin in human MSC lines. (D) Correlation between the differentiation efficiency into cardiomyocytes and cell surface N-cadherin expression in human MSC lines. The vertical axis represents the differentiation efficiency. The horizontal axis represents cell surface expression of N-cadherin. The correlation coefficient (r) is shown on the graph. $^*P < 0.05$.

expression of various cell surface proteins, which are essential for the development of the heart *in vivo* or are specifically expressed in cardiovascular progenitor cells, was examined by immunoblotting (Fig. 1B). Among these markers, the expression of N-cadherin showed a good correlation with the differentiation efficiency toward beating cardiomyocytes. The MSC lines highly expressing N-cadherin showed higher differentiation ability toward cardiomyocytes. Flk-1 also showed an expression pattern similar to that of N-cadherin. However, the expression levels in human MSCs were very low. Only an extremely long exposure (30 min) enabled us to detect the Flk-1 protein bands (Fig. 1B). The expression of c-Kit showed some correlation with the cardiomyogenic differentiation abilities of these cells, although the expression levels of c-Kit in some human MSCs that readily differentiated into cardiomyocytes were very low (Fig. 1B, UE7T-13, UE6E7T-11, and UBE6T-15).

Other cell surface proteins have been reported as essential for heart development. Integrin α4 is essential for the development of the heart and placenta [11]; a homozygous null mutant of integrin α4 caused embryonic lethality due to defects in the epicardium and coronary vessel development, leading to cardiac hemorrhage, in addition to failure of fusion between the allantois and chorion during placentation. Knockout mice of vascular cell adhesion molecule 1 (VCAM-1) displayed a reduction in the compact layer of the ventricular myocardium and intraventricular septum [12]. Platelet-derived growth factor receptor α (Pdgfrα) is expressed in cardiac progenitor cells in the posterior part of the secondary heart field. Pdgfrα is also expressed in the valves and pericardia of the heart at E12.5–16.5 [13]. However, the expression of these cell surface proteins did not show a strong correlation with the differentiation ability of human MSCs into cardiomyocytes (Fig. 1A and B).

Next, we verified the cell surface-specific expression of N-cadherin, Flk-1, and c-Kit in living MSCs by flow cytometry. Flk-1 was barely detectable on the cell surface of human MSCs (Fig. 2A), although a positive control, HUVEC, showed strong cell surface expression of Flk-1 (Fig. 2A, right), indicating that human MSCs do not express detectable amounts of Flk-1 on the plasma membrane. The cell surface expression of c-Kit was also relatively low (Fig. 2B), and the MSC lines with higher differentiation ability toward cardiomyocytes did not show a significant amount of cell surface expression of c-Kit (Fig. 2B, UE7T-13).

By contrast, N-cadherin was readily detectable in the human MSC lines with high differentiation ability toward beating cardiomyocytes (Fig. 2C). When the cell surface expression of N-cadherin (Fig. 1C) and the differentiation ability into beating cardiomyocytes (Fig. 1A) were compared with human MSC cell lines, a strong correlation was observed between these 2 events ($r = 0.81$; Fig. 1D). Immunofluorescence analysis of the human MSC line EPC-214, which readily differentiated into cardiomyocytes, showed characteristic localization of N-cadherin in cell-to-cell contacts in addition to the uniform expression on the plasma membrane (Fig. 2D). However, UE7T-9 cells, which expressed N-cadherin at low levels and did not differentiate into cardiomyocytes, did not show significant expression of N-cadherin (Fig. 2D, right). These results suggest that N-cadherin could be a good prospective cell surface marker of cardiomyogenic human MSCs.

Next, we validated the expression of N-cadherin with various primary human MSCs. Human bone marrow-derives MSCs (BMSCs) cultured for a limited number of passages gave a good correlation between the cell surface expression of N-cadherin and the differentiation ability into beating cardiomyocytes (Fig. 3A and B). Human MSCs derived from adipose tissue (ASCs) also showed similar results (Fig. 3D and E). The Pearson's correlation coefficients of cell surface expression of N-cadherin and differentiation efficiency toward beating cardiomyocytes in BMSCs and ASCs were good in both cases (0.55 and 0.77, respectively; Fig. 3C and F). As for c-Kit, we failed to detect significant expression of c-Kit in primary MSCs that showed distinct cardiomyogenic differentiation abilities (Fig. S2, 36_2). c-Kit protein could be detected on the cell surface of some primary ASCs (Fig. S2B, 1212). However, the isolation of c-Kit-positive cells from these primary ASCs was not successful by flow cytometry.

To determine whether the N-cadherin-positive population of human MSCs has higher differentiation ability into cardiomyocytes than N-cadherin-negative MSCs, we established the separation conditions of N-cadherin-positive cells using MACS (Fig. S3). Then, the N-cadherin-positive fraction was concentrated from a primary culture of human ASCs (1212 used in Fig. 3) using the same method (Fig. 4A); these cells were further cultured on mouse embryonic heart feeder cells for 7 days. The enriched ASC fraction expressing cell surface N-cadherin showed a 4-fold higher cardiomyogenic differentiation ability than the N-cadherin-negative fraction (Fig. 4B).